小脳発生における顆粒細胞移動とプルキンエ細胞樹状突起選択の計算モデル

OKINAWA INSTITUTE OF SCIENCE AND TECHNOLOGY
GRADUATE UNIVERSITY

Thesis submitted for the degree

Doctor of Philosophy

A Computational Model of Granule Cell Migration and Purkinje Cell Primary Dendrite Selection During Cerebellar Development

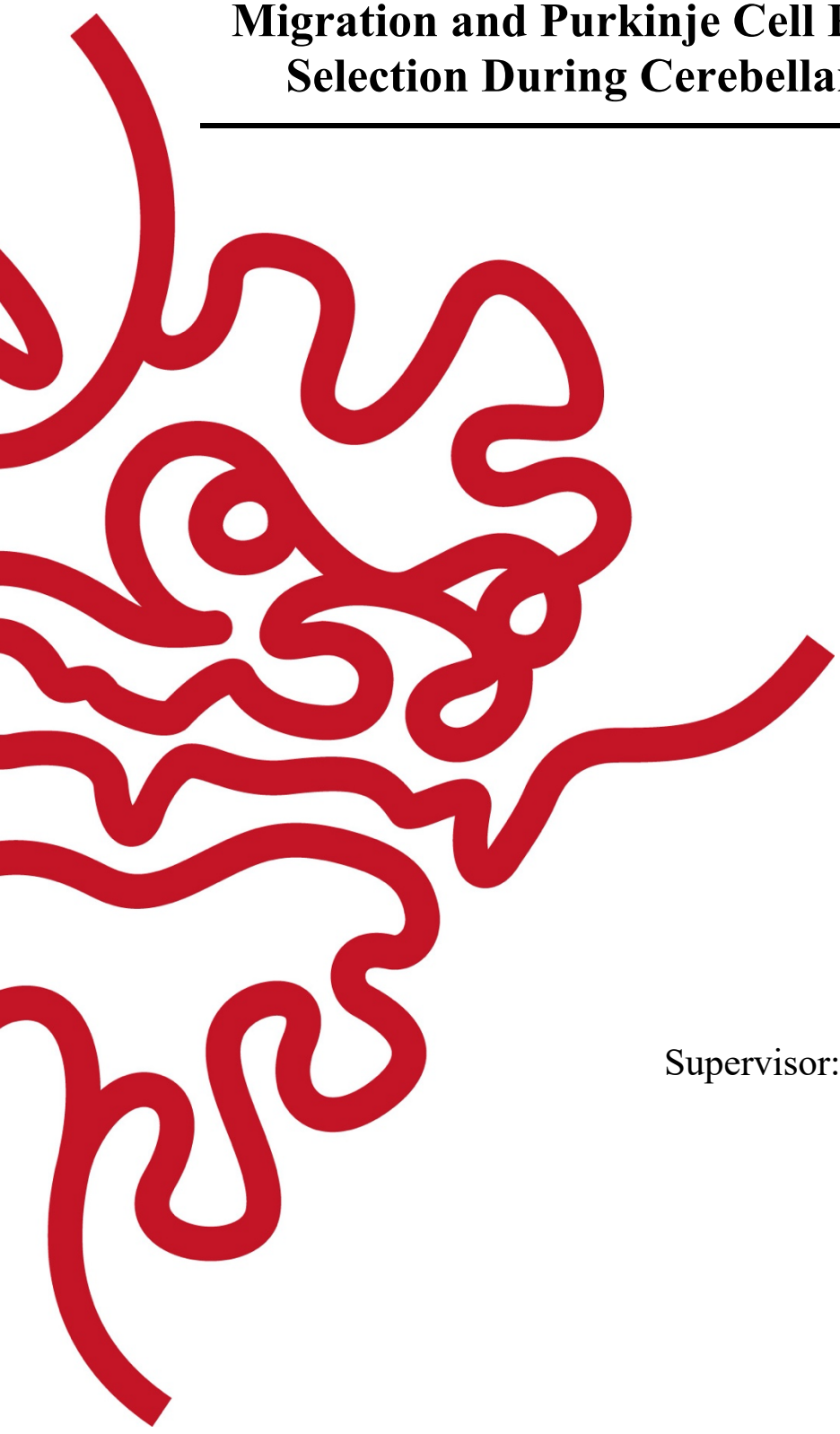

by

Mizuki Kato

Supervisor: **Prof. Erik De Schutter**

October 2022

Declaration of Original and Sole Authorship

I, Kato Mizuki, declare that this thesis, entitled, *A Computational Model of Granule Cell Migration and Purkinje Cell Primary Dendrite Selection During Cerebellar Development*, and the data presented herein are original and my own work.

I confirm that:

- No part of this work has previously been submitted for a degree at this or any other university.
- The work of others has been clearly acknowledged. Quotations from the work of others are clearly indicated, and attributed to them.
- In cases where others have contributed to part of this work, such contributions have been clearly acknowledged and distinguished from my own work.
- None of this work has been previously published elsewhere.

Date: October 18th, 2022
Signature:

Abstract

This project aims to investigate the interrelationship between primary dendrite selection of Purkinje cells and migration of their pre-synaptic partner granule cells during cerebellar development. During development of the cerebellar cortex, each Purkinje cell grows more than three dendritic trees, among which a primary tree is selected to develop further, whereas others completely retract. Experimental studies suggested that this selection process is coordinated by physical and synaptic interactions with granule cells. However, technical limitations hinder a continuous observation on multiple populations of the cells. To reveal the mechanism underlying this selection process, we constructed a computational model of dendritic development and granule cell migration, using a new computational framework, NeuroDevSim. Comparisons of the resulting morphologies from the model demonstrated the roles of the selection stage in regulating the growth of the selected primary trees. This thesis presents the first computational model that simultaneously simulates growing Purkinje cells and the dynamics of granule cell migration, revealing the role of physical and synaptic interactions upon dendritic selection. Development of the model is expected to provide new insights in the development of neonatal Purkinje cells and help to track down how cerebellar cortex develops into a normal or abnormal structure.

Acknowledgment

First and foremost, I would like to express my sincere thanks and gratitude to my supervisor Prof. Erik De Schutter for providing more than perfect support during my Ph.D. study. I am grateful for the devotion of his time and energy to bring me how far I have come. I have been very fortunate that I could have invaluable experience to learn from his coding, editing, and our weekly meetings, which I will treasure for the rest of my life. I would like to appreciate all the members of the Computational Neuroscience Unit at OIST for their support in my lab rotation and insightful feedback on the rotation project and the presenting one. I am also indebted to Okinawa Institute of Science and Technology Graduate University for providing me an opportunity to work on this project in a neat and secure environment. I sincerely appreciate Prof. Michisuke Yuzaki at Keio University and Prof. Yukari Takeo at Stanford University for sharing their invaluable data and kindly showing me the experiments on real cerebellum in their lab. I deeply thank my thesis committee members Prof. Hiroyuki Ishikawa and Prof. Marylka Yoe Uusisaari for their considerate advice throughout my Ph.D. research. I would like to express my gratitude to Prof. Goodhill J. Geoffrey and Prof. Mineko Kengaku for their time and effort serving as my thesis examiners. Finally, I would like to express my special thanks and gratitude to my family and friends for their warm encouragement. I especially appreciate enormous support from my husband, Dr. Po-Shun Chuang, for helping me to survive my Ph.D program.

Abbreviations

EGL external granule layer
ML molecular layer
PCL Purkinje cell layer
IGL internal granule layer
P postnatal days
E embryonic days
GC granule cell
PC Purkinje Cell
BG Bergmann glia

Contents

DECLARATION OF ORIGINAL AND SOLE AUTHORSHIP III
ABSTRACT V
ACKNOWLEDGMENT VII
ABBREVIATIONS IX
CONTENTS XI
LIST OF FIGURES XIII
LIST OF TABLES XV
1. INTRODUCTION 1
1.1. IMPORTANCE OF THE CEREBELLUM 1
1.2. MATURE CEREBELLAR CORTEX IN MICE 2
1.3. ISSUES IN STUDYING CEREBELLAR DEVELOPMENT 3
1.4. DEVELOPMENT OF THE CEREBELLAR CORTEX 5
1.5. PROJECT SUMMARY 10
2. METHODS 11
2.1. SOFTWARE: NEURODEVSIM 11
2.2. GRANULE CELL MIGRATION MODEL 12
2.3. EXTENDED GRANULAR LAYER MODEL 17
2.4. PURKINJE CELL MODEL 18
2.5 DATA ANALYSIS 25
3. RESULTS 29
3.1 RESULTS FROM THE GRANULE CELL MIGRATION MODEL 29
3.2. RESULTS FROM THE EXTENDED GRANULE CELL MIGRATION MODEL 35
3.3. RESULTS FROM PURKINJE CELL MODEL 37
4. DISCUSSION 52
4.1. SUMMARY OF THE MAIN RESULTS 52
4.2. LIMITATIONS OF THE MODELS 53
4.3. POTENTIAL IMPROVEMENTS AND FUTURE DIRECTIONS OF THE MODELS 53
4.4. CONTRIBUTIONS OF THE MODELS 54
BIBLIOGRAPHY 56

List of Figures

Figure 1. Mature mice cerebellum 2
Figure 2. Changes in layering structure during the development in the cerebellar cortex.. 6
Figure 3. Stage of the dendritic development in mice 8
Figure 4. Granule cell model. 13
Figure 5. Extended granule cell model 17
Figure 6. Criteria for Success. 26
Figure 7. Purkinje cells to be analyzed 28
Figure 8. Simplified code structure for modeling granule cell behaviors 29
Figure 9. Results from the representative granule cell model. 31
Figure 10. Example cases for granule cells that got stuck during migration or extensions 34
Figure 11. Extended granule cell model 36
Figure 12. Characteristics of 3 growth scenarios 38
Figure 13. Arbor size of winner trees 40
Figure 14. Morphology of winner trees by z-area. 42
Figure 15. Number of synapses and arbor size of winner trees from retraction scenarios 45
Figure 16. Morphology of winner trees by three z-area in retraction scenarios 47
Figure 17. Change in path length with increasing cycles 48
Figure 18. Morphology of individual winner trees from single samples in retraction scenarios. 49
Figure 19. Variability of winner tree size in retraction scenarios 50

List of Tables

Table 1. Comparisons of the three retraction scenarios..... 24
Table 2. Description of each mode status in the granule cell model..... 30
Table 3. Descriptions of each method in granule cell model. 30

1. Introduction

1.1. Importance of the cerebellum

1.1.1. Cerebellum and diseases

The cerebellum plays important roles in both motor and non-motor functions. Deficits during cerebellar development affects cognitive capabilities and leads to psychiatric disorders such as schizophrenia, autism spectrum disorders, or ADHD (Butts, Green, & Wingate, 2014; Limperopoulos et al., 2007; Manto, Gruol, Schmahmann, Koibuchi, & Rossi, 2013; Tavano et al., 2007).

1.1.2. Structural features of the cerebellum

The cerebellum comprises only 10% volume of the whole brain but holds more than 70% of neurons in the mammalian brain. Most of these neurons are densely packed cerebellar granule cells whose population is too numerous to be counted (estimated densities can range from 500,000 (Zanjani, Vogel, Delhaye-Bouchaud, Martinou, & Mariani, 1997) to 6,562,500 (Steen, 2006) cells per mm^3 in mice, compared in (Keller, Erö, & Markram, 2018). Despite the numerical predominance of its neurons, the cerebellum is sometimes referred to as simpler than the cerebrum. This is partially because outputs from the cerebellar cortex are composed of a single type of neuron, the Purkinje cell. Mature Purkinje cells are one of the largest neurons in the brain and are characterized by a planar structure of their dendritic trees. Each dendritic tree receives excitatory synapses from over 100,000 parallel fibers (axons of granule cells), and a single climbing fiber, which serves as an afferent to the cortex from the inferior olivary nuclei in the medulla.

1.1.3. Conserved cerebellar development in mice and human

Given the highly conserved structure of the cerebellum within vertebrates and the fact that they share similar developmental courses, rodent models such as mouse and rat have been widely used in experimental studies of the cerebellum. Compared to the cerebellum in mice, the human cerebellum is much larger and its development proceeds slower (Zecevic & Rakic, 1976). For example, in both mouse and human cerebella, granule cell precursors first accumulate at a temporal layer (the external granular layer), and migrate to the destined place (internal granular layer) afterward. This occurs during birth to third postnatal weeks in mice (Komuro, Yacubova, Yacubova, & Rakic, 2001; Leffler et al., 2016; Miale & Sidman, 1961; Constantino Sotelo, 2004), but during 30-week gestation to 18 postnatal months in human (Gadsdon & Emery, 1976; Leffler et al., 2016). Similarly, differences are also observed for the development of Purkinje cells in mouse and human cerebella. For example, the morphological remodeling of Purkinje cells from a stellate shape to a mature shape, referred as the third stage of Purkinje cell development (Ramón Y Cajal, 1911), has been observed between postnatal day 4 to postnatal day 20 in mice (C Sotelo & Dusart, 2009; Weiss & Pysh, 1978), and between 28-week gestation to first

postnatal year in human (Miyata, Miyata, Mikoshiba, & Ohama, 1999; Zecevic & Rakic, 1976).
Therefore, the mouse cerebellum can be considered as a smaller and faster developing version of the human cerebellum in these aspects and constitutes a useful objective for getting a more detailed understanding of the human cerebellum.

1.2. Mature cerebellar cortex in mice

The cerebellum is subdivided into 10 lobules by fissures running perpendicular to the anterior (ant) to posterior (pos) axis (Figure 1A). From the developmental perspective, lobule I and X mature earlier than lobules VI, VII, and VIII (Altman, 1972). The cerebellar cortex has a well-organized layer structure. These start from the molecular layer at the top, Purkinje cell layer in the middle, and granule cell layer at the bottom of the cortex. Then, white matter comes below the granule cell layer (bottom right panel of Figure 1A & indicated on the right side of Figure 1B). The cerebellar cortex contains two different types of neurons: glutamatergic neurons (excitatory) and GABAergic neurons (inhibitory) (Altman, 1997; Ito, 2006; Squire et al., 2012). The circuit in the cerebellar cortex is regulated by several types of neurons (Figure 1B), and its Purkinje cells are the only output from the cortex. Purkinje cells receive two types of excitatory inputs, from parallel fibers and from climbing fibers. Purkinje cells project inhibitory outputs to cerebellar nuclei which also receive collateral input from afferents to the cerebellar cortex (climbing fibers and mossy fibers, Figure 1B).

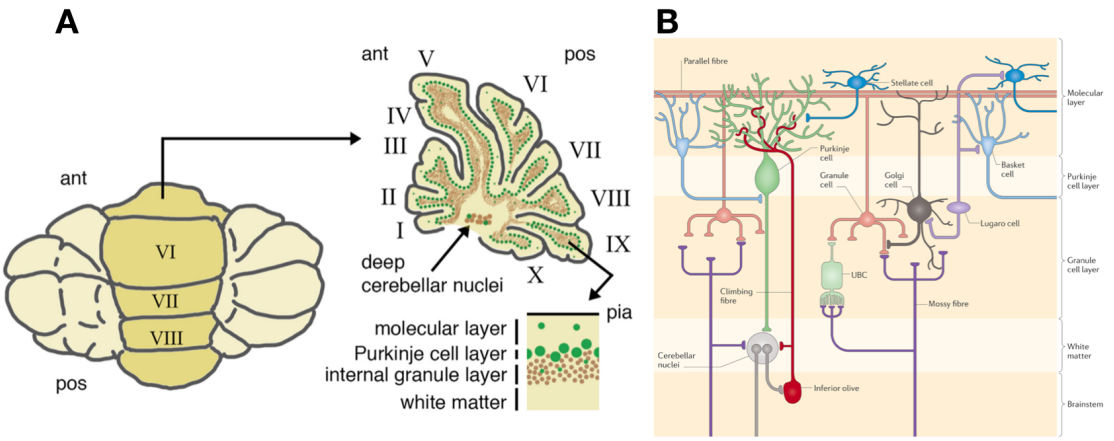

Figure 1. Mature mice cerebellum. A) A schematic representation of a whole and parasagittal slice view of mature mice cerebellum. GABAergic neurons are labeled with green, and glutamatergic ones are in beige (Basson & Wingate, 2013). B) Simplified description of neuronal circuit in mature cerebellum in 2D (Cerminara, Lang, Sillitoe, & Apps, 2015). Granule cells and unipolar brush cells (UBCs) are glutamatergic neurons. Purkinje cells, interneurons in the molecular layer (basket and stellate cells), and interneurons in the granule cell layer (Golgi and Lugaro cells) are GABAergic neurons.

1.3. Issues in studying cerebellar development

1.3.1. Technical challenges in experimental studies

1.3.1.1. Existing in vivo time-lapse analysis

Purkinje cells have been widely employed as neuronal models to investigate dendritic differentiation, with established immunohisto-chemical and genetic manipulation techniques (Leto et al., 2016; Nishiyama et al., 2012).
By analyzing time-lapse pictures of target neurons taken at different time points (e.g. every 10 hours), a previous in vivo study demonstrated development time course of Purkinje cells. The target neurons were observed through an imaging window opened at the skull of a P6 mouse above the cerebellar cortex, which enables in vivo observation until the skull grows back.

1.3.1.2. Technical limitations to obtain in vivo time-lapse images

However, in vivo time-lapse images of early postnatal animals are not always readily available, due to technical difficulties and animal related issues. For example, surgeries for implanting imaging windows for the time-lapse imaging are challenging because postnatal tiny animals are delicate, which limits the number of samples that can be obtained from these experiments. Low survival rates of pups after the surgery constitutes another problem. Further adding to the complexity, pups survive the operations are often killed or eaten by their mothers or foster mothers (personal communication, Prof. Yukari Takeo and Prof. Michisuke Yuzaki). Also, it should be noted that development varies in different places among Purkinje cells and cannot be just categorized by postnatal days. Late developing lobules like VI, VII, and VIII show earlier developmental stages than Purkinje cells in other lobules at the same postnatal day. Different developmental stages can also coexist in the same lobule or within neighborhoods (Armengol & Sotelo, 1991). These variabilities make it difficult to generate robust representatives of dendritic morphologies. As a consequence, the exact flow of the developmental discontinuities in Purkinje cell morphogenesis is still largely unclear.

1.3.2. Limitations in existing computational models

1.3.2.1. Computational models to complement experimental methods

Computational models for neuronal developments have emerged as complementary tools to experimental approaches. By converting complex biological factors into more generalized parameters, computational models provide alternative means to test hypotheses arisen from experimental data. These models can also provide new interpretations of experimental data and inspire new experimental approaches (Brodland, 2015).

1.3.2.2. Mechanistic computational models

In neural science, some computational models have attempted to simulate neuronal development based on biological mechanisms. Such mechanistic computational models

establish plausible connections with real systems. Unfortunately, computational modeling of neural development is still in its infancy as most mechanisms of neuronal development are not fully understood, which constrains availability of model parameters. Furthermore, including all revealed biological mechanisms in a single computational model is technically challenging for common computational devices. Even with devices of sufficient computational powers, the level of abstraction or complexity of a model should be chosen carefully so that the model can reasonably describe mechanisms of interest. Also, finding parameters or constraints of the parameters that describe the molecular mechanisms can be a big hurdle for mechanistic models.

1.3.2.3. Three mechanisms to be modeled

Because of these hurdles, most computational models only focus on particular biological phenomena. Modeling dendritic selection of Purkinje cells with environmental interactions necessitates understandings of mechanisms underlying axon guidance, migration, and dendritic growth. These three mechanisms mediate environmental information through a common structure, growth cones, in real biological system. However, previous computational models for these three phenomena were developed independently.

1.3.2.4. axon guidance models

The growth cones are intensively instantiated in axon guidance models. Major contexts chosen for simulating the axonal guidance are mostly 2D (Forbes, Thompson, Yuan, & Goodhill, 2012; Fraser & Perkel, 1990; Goodhill, Gu, & Urbach, 2004; Simpson & Goodhill, 2011) or dimensionless for molecular diffusion models (Graham, Lauchlan, & Mclean, 2006; McLean, van Ooyen, & Graham, 2004). Few exceptions can be found (Roccasalvo, Micera, & Sergi, 2015), but the model is specialized to demonstrate specific behavioral responses of axonal growth cones. It may be appropriate to simulate complex axonal guidance in lower dimensions.

1.3.2.5. migration models

In contrast to the preference to low-dimensional context in axon guidance models, migration models rely more on a 3D context (Frascoli, Hughes, Zaman, & Landman, 2013; Zaman, Kamm, Matsudaira, & Lauffenburger, 2005). In migration models, concept of a leading process is barely considered because most migration models were developed for tumor cells instead of neurons (Merino-Casallo, Gomez-Benito, Juste-Lanas, Martinez-Cantin, & Garcia-Aznar, 2018; Paňková, Rösel, Novotný, & Brábek, 2010; Ribeiro, Gómez-Benito, Folgado, Fernandes, & García-Aznar, 2017; Talkenberger, Cavalcanti-Adam, Voss-Böhme, & Deutsch, 2017; Zhu & Mogilner, 2016). Although how tumor cell migration models simulate different types of migration can inspire migratory modes of cerebellar granule cells, most tumor models focus on extracellular matrix interactions rather than those between different cell types.

1.3.2.6. dendritic growth models

Dendritic growth models simulate stepwise growth of dendritic trees. Most mechanistic dendrite growth models have focused on intrinsic cellular factors, such as tree morphology itself or intracellular molecular transport (van Pelt, Graham, & Uylings, 2003). A few exceptions simulate extrinsic factors such as neurotrophic molecular gradients or self-avoidance of dendrites of the same cell (Luczak, 2006). CX3D is a modeling software capable of simulating neuronal development in a 3D space based on both intrinsic and extrinsic factors (Zubler & Douglas, 2009). However, simulation with CX3D is memory intensive. More importantly, there have been no recent updates to the software. New computational approaches are therefore needed for a better understanding the role that granule cells play in the early developmental stage of Purkinje cells. It should be noted that often compromises between implementations of the different phenomena need to be made to make modeling possible.

1.4. Development of the cerebellar cortex

1.4.1. Layering change during development by granule cell migration

During cerebellar development, granule cell precursors first proliferate in the outermost area of the cortex to form a temporal layer (the external granule layer (EGL)) right above the molecular layer (Figure 2A: P0 and P6). As the cerebellum develops, massive numbers of granule cell precursors firstly accumulate and proliferate at the external granule layer. During differentiation into granule cells, they slowly move to the bottom of the external granule layer while extending future parallel fibers in tangential directions in the molecular layer. Their migration down the molecular layer occurs along the palisade-like structure of Bergmann glia processes (Figure 2B). These migrating granule cells eventually penetrate through the Purkinje layer, and form the internal granule layer (IGL) at the bottom of the cortex (Figure 2A: P12 and P19). In mice, this layer swapping process completes around P15 or in the third postnatal week (Komuro et al., 2001; Miale & Sidman, 1961; Constantino Sotelo, 2004).

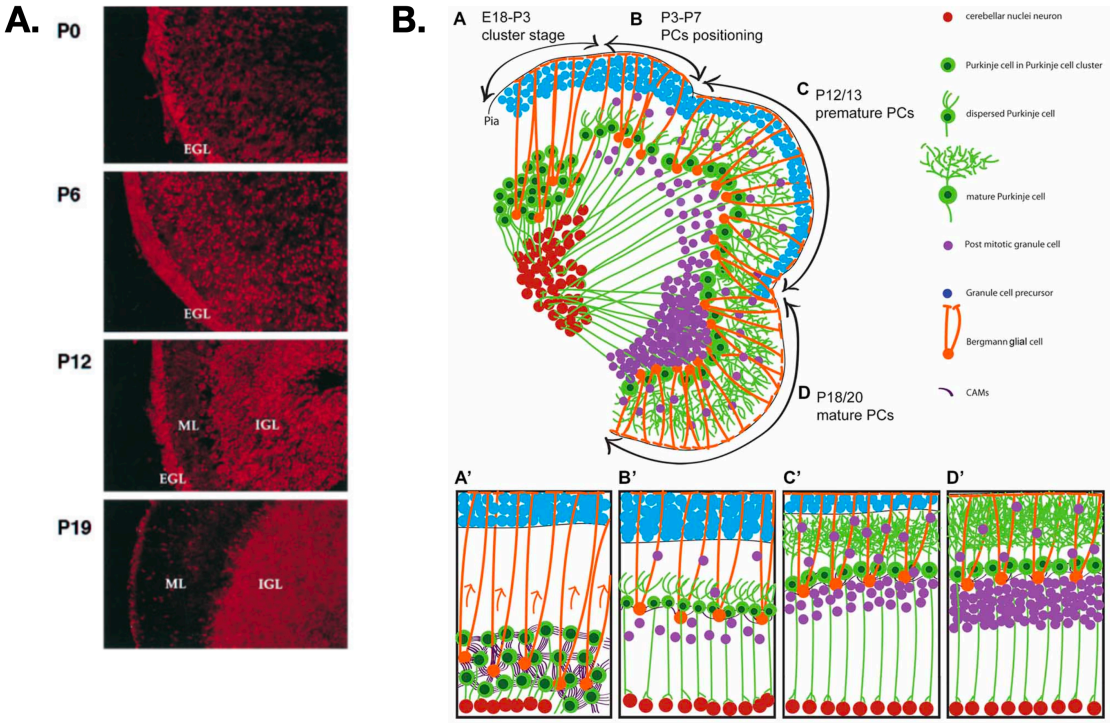

Figure 2. Changes in layering structure during the development in the cerebellar cortex. A) Visualization of granule cell migration on sagittal section of rat cerebellum showing dynamic layering rearrangement in the cortex. Granule cells are stained with red antibodies (modified from Rio, Rieff, Qi, and Corfas (1997)). EGL: External granule layer. ML: Molecular layer. IGL: Internal granule layer. B) Schematic drawing of radial migration of post-mitotic granule cells (purple balls) along the Bergmann glia process (orange fibers) in mice (Rahimi-Balaei, Bergen, Kong, & Marzban, 2018). Different areas of the sagittal slice of cerebellum depict varied period of the development. In area A (zoomed in on panel A'), granule cell precursors (blue dots) accumulated at the surface of the cortex while Purkinje cells (green) are migrating upwards along with Bergmann glia. Red dots in the bottom are cerebellar nuclei where axons of Purkinje cells project. In area B and panel B', Purkinje cell are aligned to form a Purkinje cell layer. The granule cell precursors germinate to make ticker external granule layer and post mitotic granule cells (purple) started their radial migrations. In area C and C', more and more granule cells migrate radially and accumulate beneath the Purkinje cell layer as granule cell layer. The Purkinje cells have extended their dendritic trees. In area D and D', external granule cell layer is gone as all granule cells have left the germinal zone. CAMs: Cell Adhesion Molecules.

1.4.2. Dendritic development of Purkinje cells

1.4.2.1. Stages of dendritic remodeling

Another event happening during cerebellar development is maturation of Purkinje cells. Evidence from murine cerebellum show that Purkinje cell somas settle in the Purkinje cell layer around birth and go through multiple remodeling stages in the first postnatal week (Figure 3), including:

① A simple fusiform stage, in which a Purkinje cell presents a tear drop-like soma with a single long, thin dendrite (Armengol & Sotelo, 1991);
② A complex fusiform stage, in which a Purkinje cell shrinks the single long dendrite and develops several thin dendrites from the sides (Armengol & Sotelo, 1991);
③ A non-dendritic stage, in which a Purkinje cell retracts all presenting dendrites (Armengol & Sotelo, 1991);
④ A stellate stage, in which a Purkinje cell forms a stellate shape by growing new dendrites again from the soma (Ramón Y Cajal, 1911);
⑤ A dendrite-selection stage, in which a Purkinje cell retracts some newly formed dendrites once again, leaving 5 to 6 thick candidate dendrites sticking out around the top side of the soma (C Sotelo & Dusart, 2009);
⑥ A young Purkinje cell stage, in which a Purkinje cell selects one (or sometimes two) of the candidate dendrites as a primary dendrite and retracts the unselected ones (C Sotelo & Dusart, 2009);
⑦ A tree-growing stage, in which selected dendrite(s) further develop to a mature structure (Ramón Y Cajal, 1911).

Within this discontinuous, non-linear developmental course, we are interested in the dendrite-selection stage. The selection stage looks like an extra stage in the tree development which can be hypothesized as either an important step to attain, for example, a primary tree with most efficient morphology for developing neuronal network or an inefficient step to be eliminated in the future by evolution.

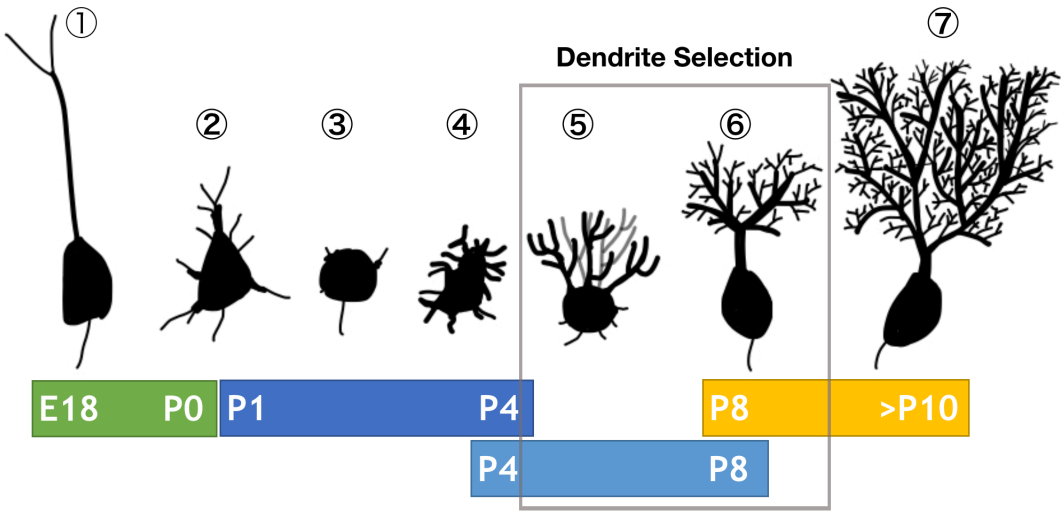

Figure 3. Stage of the dendritic development in mice. Schematic drawing of the seven stages of Purkinje cell dendritic development: ① Simple Fusiform Stage, ② Complex Fusiform Stage, ③ Devoid of Dendrite Stage, ④ Stellate Stage, ⑤ Primary Dendrite Selection Stage, ⑥ Young Purkinje Cell Stage, ⑦ Tree Growth Stage. The embryonic (E) and Postnatal (P) days on the bottom are roughly estimated periods that each stage is often observed.

1.4.2.2. Intrinsic mechanism for retracting dendritic trees

The earlier remodeling stages (① to ④) are most likely driven by intrinsic mechanisms of Purkinje cells, as they are not hindered by the absence of climbing fibers in vitro (Boukhtouche et al., 2006; Poulain et al., 2008) or by the absence of granule cells in vivo (stagger and weaver cerebella (Berry & Bradley, 1976). Some intrinsic systems of Purkinje cells still govern basic retraction mechanisms in the initial screening of dendrites at a stellate stage. For instance, dendritic retractions at a stellate stage were observed in vitro in isolated Purkinje cells upon physical collisions between growing dendrites of the same cell (Fujishima, Horie, Mochizuki, & Kengaku, 2012). Also, retraction of shorter and less branched dendrites suggests simple retraction rules governed by some intrinsic factors (Tanaka, Yanagawa, Obata, & Marunouchi, 2006). However, isolated Purkinje cells do not fully retract excessive dendritic trees in in vitro conditions, resulting in a state of multiple primary dendrites (Fujishima et al., 2012; Tanaka et al., 2006). These findings suggest that the final screening of primary dendrites in the dendrite-selection stage depends on environmental factors.

1.4.2.3. Environmental factors involved in the dendrite-selection stage

1.4.2.3.1. Climbing fibers and mossy fibers

Climbing fibers and mossy fibers, two afferents to the cortex, form synapses with developing Purkinje cells during the dendrite-selecting stage (Altman, 1972; Takeda & Maekawa, 1989). Climbing fibers are involved in organizing the final shapes of Purkinje cell dendrites (Berry & Bradley, 1976). An in vivo study demonstrated a reduced branching pattern in dendritic arborizations of Purkinje cells in rats, when climbing fibers were removed by thermocoagulation (C Sotelo & Arsenio-Nunes, 1976). Similarly, transient contacts of mossy fibers with developing Purkinje cells are likely involves in assembly of zonal circuit maps of the cerebellum (Kalinovsky et al., 2011; Sillitoe, 2016).

1.4.2.3.2. Granule cells

Another candidate for neuronal interactions with Purkinje cells are granule cells, which have been recognized as having a close relationship with dendritic arborizations of Purkinje cells (Blazeski & Mason, 1994; Morrison & Mason, 1998). As described earlier, intensive migration of granule cells happens next to the developing Purkinje cell dendrites during the dendrite-selection stage. Earlier studies have captured physical proximity of vertical leading processes extended from granule cells and dendrites of Purkinje cells during cerebellar development under microscopic observations (Das, Lammert, & McAllister, 1974; Ono et al., 1997). At a molecular level, crosstalk between developing Purkinje cells and migrating granule cells are crucial for proper alignments of both neurons and for dendritic arborization of Purkinje cells (Otero et al., 2014). Specifically, synaptic interaction through NMDA receptors is thought essential for dendritic retractions of Purkinje cells (personal communication, Prof. Yukari Takeo), which is a critical process during the dendrite-selection stage. Given their proximity, the parallel fibers and ascending axons of migrating granule cells growing next to developing Purkinje cell dendrites are the most likely source of such synaptic interaction. Supportingly, global disturbance of post-synaptic GluD2 receptors, which are involved in synaptogenesis between parallel fibers and Purkinje cell dendrites, strongly impacts Purkinje cell morphology in mice, including the number of primary dendrites at P7 (Takeo et al., 2021). These findings suggest granule cells as strong candidates to contribute to the final selection of primary dendrites of Purkinje cells, via either or both physical interactions and molecular signaling. However, the interactions between granule cells and Purkinje cells in this stage have not yet been investigated in detail.

1.5. Project Summary

The aim of this project is to investigate the relationship between Purkinje cell's primary dendrite selection and granule cell migration during cerebellar development by constructing a computational model. This model is the first attempt to simulate development of the cerebellar cortex with detailed physical and synaptic interactions between different types of its main neurons. It was built from scratch and serves as a prototype cerebellar developmental model compromising modeling granule cells and Purkinje cell together. The model provided new insights about the distinct planner morphology of Purkinje cell dendrites and about roles of the dendritic selection process during the cerebellar development. The model also supports hypothesis that synaptic interactions by granule cells are likely to be involved in the selection procedure.

2. Methods

2.1. software: NeuroDevSim

2.1.1. main properties of NeuroDevSim

2.1.1.1. features of NeuroDevSim

I used the NeuroDevSim software (De Schutter, 2022), evolved from NeuroMaC (Torben-Nielsen & De Schutter, 2014) to construct and simulate the model. NeuroDevSim is a computational framework that enables users to model stepwise stochastic 3D growth of neuronal morphologies over given simulation cycles. The specialty of this software is its focus on simulating phenomenological interactions with the environment for shaping neuronal structures. In other software for modeling dendritic growth, environmental influence is restricted to extracellular substrates or repulsions between dendrites from the same neurons. NeuroDevSim is only the active software that can additionally represent simultaneous interactions with populations of different types of neurons. NeuroDevSim can be imported as a python module and run in a multi-core computing environment. Simulations can be run as a Python process in jupyter notebooks with interactive graphic output or from the terminal. Simulation data is saved in SQL datatype format, and can be extracted to generate off-line plots or movies using provided functions, and to analyze the data set. Simulations were executed on the High-performance computing cluster Deigo at OIST, using AMD Epyc 7702 CPUs with 128 cores and 512GB memory. 64 cores are used for each simulation.

2.1.1.2. Fronts as agents

NeuroDevSim represents stepwise growth of neuronal structures by agents called fronts, which are inspired by biological growth cones. In physiological development, growth cones elongate, branch, terminate, or retract. They can lead migration of the cell's soma by sensing local extracellular molecules (Itoh et al., 1993; Jan & Jan, 2010). In NeuroDevSim, each front can individually follow their own growth rules for elongation, branching, termination, retraction, and migration according to provided surround information. Each active front takes a single action per cycle (e.g. adding certain length of new front at the tip = elongation), which makes one cycle equivalent to a time frame ranging from a few minutes to hours or more.

2.1.1.3. interpretations of phenomenological rules

In actual coding, users can generate growth rules defined by topological features (e.g. changing branching probability depending on centrifugal orders). Unlike other topological rule-based software or mathematical models, fronts only receive limited information about the distal environment so that it follows the biological assumption that growth cones obtain information only from their direct surrounds. NeuroDevSim can additionally implement stochastic detection of nearby chemical cues for attraction or

repulsion. However, the rules purely defined by topological features can also be interpreted with intercellular mechanisms such as competition for available resources or messenger molecules within cells. Synaptic interactions between neurons can be simulated in NeuroDevSim. Due to the time scale of simulation cycles, it does not implement processes occurring in milliseconds (e.g. voltage change etc.) but it can represent synaptic weight or average firing rate. Intracellular release of signaling molecules in dendrites of axons based on these synaptic interactions can also be implemented, which can be additional factors to regulate extensions or retractions of neuronal structures.

2.2. Granule cell migration model

Due to the availability of larger experimental data and more opportunities to have follow-up experiments, the mouse is selected as a model organism to construct the computational model for this study. The model embodies the Purkinje cell layer and the molecular layer. Its Purkinje cell layer has somas of Purkinje cells and Bergmann glia. The molecular layer has simplified Bergmann processes for guiding granule cells and migrating granule cells which gradually fill up the layer with their descending axons and parallel fibers.

2.2.1. The model structure at initiation phase

2.2.1.1. Simulation cube

The simulation of the granule cell migration is performed in a (x1, y1, z1), (x2, y2, z2) = (-20, -20, -20), (180, 160, 140) μm^3 cube, representing a part of a murine cerebellar cortex (lobule VI) around postnatal days 0 to 10. The x-axis of the cube represents sagittal plane, y-axis represents transversal plane (long axis of folium), and z-axis is the depth of the cerebellar cortex (Figure 4A and B). Placement of Purkinje cell somas were calculated from (x, y, z) = (0,0,0), and the simulation cube itself was extended to place Bergmann glia around the Purkinje cell somas.

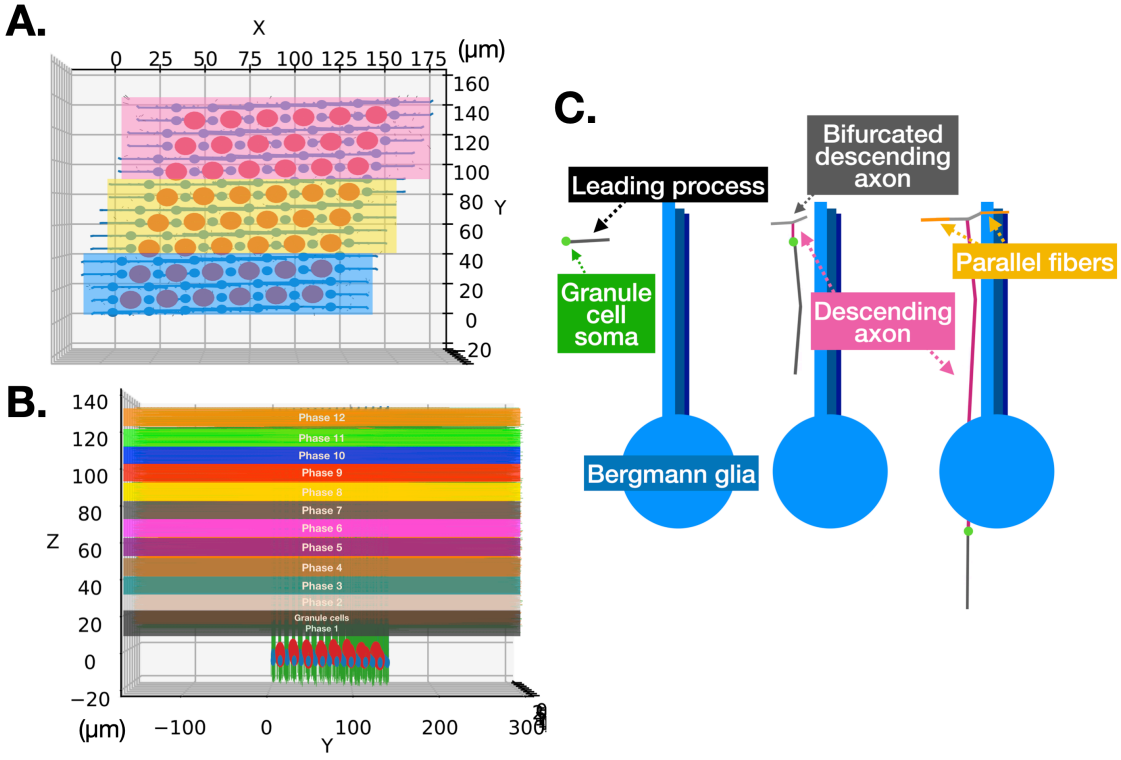

Figure 4. Granule cell model. A) Top view of the granule cell model before initiations of granule cells. Large spheres are Purkinje cell somas, and smaller blue spheres are somas of Bergmann glia which extend processes. Color-shaded rectangles shows 3 areas where granule cells are placed. B) Side view of the granule cell model after all green granule cells finish migration and color stripes represent z-locations of granule cell initiation from 1 to 12 phases. C) Schematic representation of how each granule cell migrates using a Bergmann glia process as a guide. At [1], granule cell soma (a small green dot) is horizontally migrating to one of the closest Bergmann glia processes (light blue, more distant glia processes of same cell are dark blue) by extending a cylindrical leading process (gray). At [2], the granule cell soma gets close enough to the target process, and starts radial migration by extending the leading process downwards along the process while extending an axon (pink) from the tail of soma which further bifurcate into parallel fibers. In [3], the soma keeps migrating down and parallel fibers further extend along y-axis in both directions. A line of axonal fronts lays down along the path of the radial migration of the soma.

2.2.1.2. Purkinje cell somas

In the cube, 48 Purkinje cell somas settle as spherical objects in the Purkinje cell layer ($-11 < z < 4$ μm). Each soma is 6 μm in radius, and their arrangement is according to the parallelogram soma placement observed in cat cerebella (Palkovits, Magyar, & Szentagothai, 1971). In this granule cell model, they have not yet extended dendritic trees.

2.2.1.3. Bergmann glia objects

119 Bergmann glia somas with 3 µm radius are placed in the Purkinje cell layer avoiding overlap with Purkinje cell somas. Each Bergmann glia soma extends, on average, 4 cylindrical processes. These cylindrical process fronts grow 4 µm per cycle extending towards the top surface (z = 120) of the cube. As a structure, the processes orient in palisades along the x-axis in the model as they are along the sagittal plane in murine cerebellum (de Blas & Cherwinski, 1985; De Zeeuw & Hoogland, 2015). From the top view, tips of the processes extended from different Bergmann glia somas are also aligned along the transversal plane in mice, which is mimicked in the model as much as possible. During the biological development, Bergmann glia are still mitotically active during the target phase (proliferation peaks at P6 to P9 in rats (Shiga, Ichikawa, & Hirata, 1983)). However, Bergmann glia are treated as static objects in the model because of how collisions are dealt with in the software and because the simulation volume stays the same. In the model, physical thrust or shoving between cells cannot be simulated since simulating deformation of objects is difficult in large population models. Without thrusting, it is tough to extend new Bergmann processes in a crowded molecular layer filled up with copious granule cells and their axons. In addition, tissue expansion during cerebellar development is not implemented due to technical limitations of the simulator. Therefore, there is no increase of space in the model which makes it more difficult to introduce new processes.

2.2.2. Granule cell migration algorithm

2.2.2.1. initiation of granule cell somas

The granule cell soma radius is modeled as 0.1µm, which is much smaller than the actual value. The reason is that, as mentioned above, physical shoving between cells cannot be simulated in the model, and the smaller diameter represents the ‘squeezed' soma structure of actual granule cells. After Purkinje cell somas and Bergmann glia somas are initiated in the cube and Bergmann glia processes start to extend, granule cells are randomly initiated, but with minimal separation by their diameters, in specific 3 grid areas (Figure 4A). 3,024 granule cells are gradually initiated in 12 consecutive phases: this starts from phase 1 at z-axis of 15 - 25 µm during cycle 6, phase 2 at 25 - 35 µm during cycle 16, phase 3 at 35 - 45 µm during cycle 26 and so on till phase 12: 125 - 135 µm during cycle 116 (Figure 4B).

2.2.2.2. horizontal migration (migration mode 0 to 1)

Migration mode 0

At the initiation, granule cells set as migration mode 0. They are searching nearby Bergmann glia process within a 20 µm search radius.

Migration mode 1

After finding a target glia, granule cells turn to mode 1 and start moving closer to the target Bergmann glia cylindrical front. Granule cells migrate by extending cylindrical leading processes and their somas migrate along the path that leading processes explore. The radius of the leading process is assigned as 0.1μm. In the biological system, leading processes and somas of granule cells are elastic and change their diameters and shapes to push through limited space. In the model, a radius of the leading process is the same as that of the granule cell soma as we assume that if a leading process can go through an available path, its soma can also move through that space. Granule cell somas keep migrating horizontally towards the target Bergmann glia front until the leading process reaches to the state of 'close_enough'; 0.2 μm for phase 1 to phase 3, 0.35 μm for phase 4 to 6, 0.5 μm for phase 7 to 9, and 0.65 μm for phase 10 to 12. The 'close_enough' parameter is larger for later migrating granule cells. This is because descending axons of earlier granule cells wrap around Bergmann glia processes, and later ones cannot be physically as close to the glial process without pushing the existing objects in the simulation aside.

2.2.2.3. radial migration (migration mode 2 to 5)

Migration mode 2

After getting close enough to the target Bergmann glia front, a horizontally migrating granule cell is flagged as mode 2 to prepare radial migration down along the target Bergmann glia process. This preparation includes extension of an upward axon front from the tail of the soma which will extend to become the descending axon, in addition to extending a leading process downwards.

Migration mode 3

After successful extension of a descending axon at the tail of the soma, granule cells turn to mode 3. The descending axon is generated by extending a 2.0 μm front upwards but a little away from the target Bergmann glia process to create small segregation of areas between radial soma migration and parallel fiber extension which bifurcate from the tip of the descending axon. The parallel fibers extend along the y-axis by 4 μm steps until they reach the end of the simulation cube (y = -20 or 160). At the front of the soma, it elongates a 5 μm leading front downward along the Bergmann glia process. After the leading process extends a new leading process front further down, the soma migrates onto the first leading process. The space previously occupied by the soma is occupied by a new descending axon front after the soma migrated to the connecting leading process. Then, the new leading process extends another leading process front and the soma migrates further replacing its current place with axon, and so on. A line of descending axon fronts lies along the migratory path of granule cell soma in the molecular layer (Figure 4C). During this radial migration, the leading process sometimes moves away from the guidance Bergmann glia process as a result of solving collisions with surrounding structures (most likely descending axon fronts of other granule cells). If the deflection is farther than the defined close enough distance, granule cells prioritize horizontal movement to stay close to the Bergmann glia process so that they keep the defined 'close_enough' distance.

Migration mode 4

When the leading process front tip hits z = 4 μm, the granule cell leaves the guidance of Bergmann glia processes and simply goes down by passing through gaps between Bergmann glia and Purkinje cell somas.

Migration mode 5

Finally, the radial migration stops below the Purkinje cell layer when their leading process reaches z = -15 μm. Their somas accumulate in the IGL, but the model does not represent the accumulation patterns of granule cells observed in the biological system nor does it simulate dendrite formation.

2.2.2.4. approaches for collisions

Granule cells in the model often experience collisions with surrounding structures during their migration and extensions of fibers. Two built-in methods in NeuroDevSim are used for dealing with collisions happening for leading process fronts: solve_collision() and alternate_locations(). Solve_collision() provides a bypass to reach the destined position using multiple fronts rather than hitting the point with single front. This method is especially effective for dodging large spherical objects like a Purkinje cell soma and a Bergman glia soma which block entrance of granule cells to the Purkinje cell layer. If solve_collision() still returns a collision error, the code tries to extend a front with a 1/3 shorter length. Solve_collision() is tried again with the 1/3 short length, if the shorter step does not work. Because complex collisions happen during radial migration, the code uses an additional collision solution during migration mode 3. If above 2-phased solve_collison() strategies failed and a cell is in mode 3, a cell seeks free positions around a Bergmann glia process it is migrating by using alternate_locations() method as the last resort. The alternate_location() method calculates xyz coordinates in a circle around a colliding partner with a given diameter, and check if there is an open space to get around the obstacles. If granule cells are stuck in the molecular layer, they remove themselves from the simulation cube after retracting all the extended parallel fibers, axons, and leading processes.

When it comes to extensions of parallel fibers, they encode measures specific to their colliding partners using alternative_locations(). If they collide with relatively large structures like Bergmann glia process and Purkinje cell dendrites, they seek free space in the same direction but points on circumference with radius according by the radius of a colliding partner. When they collide with structures with similar radius, like other granule cells and their parallel fibers, they try to find free positions around the colliding structure. If none of the first set of points are available, they try to extend to one more set of points on a larger circumference. If all calculated points are occupied by other structures, parallel fibers give up further extension. The code uses a different strategy for dealing with collisions occurring in root axons. If an extension of initial axon fails when it turns to the migrating mode 2, the code let the granule cell continue on its radial migration without axon and try to extend the axon again with some noise ($0.0 < x < 1.0$ away from a

migrating Bergmann glia process, $0.3 < y < 1.0$, $0.3 < z < 1.0$). If there is no chance to extend an initial axon until a granule cell reaches the Purkinje cell layer, the cell will complete the migration without its axon. Examples of granule cells failing to deal with these collisions are shown in the Results section.

2.3. Extended granular layer model

2.3.1. Extended cube and incoming parallel fibers

In the real system, parallel fibers from granule cells that migrate downward in distal areas of the cerebellar cortex extend into the simulated area. Therefore, an extended version of the granule cell migration model was also designed to generate environment for Purkinje cell dendrites to grow. This version of the model is simulated in a cube with an enlarged y-axis (x1, y1, z1), (x2, y2, z2) = (-20, -20 → -160, -20), (180, 160 → 300, 140) µm3, and incoming parallel fibers of 10296 granule cells are added. This number was calculated by anatomically known density of the cells applied to the given volume. These incoming parallel fiber structures only portray parallel fibers themselves, just a soma with 2 cylindrical fronts which extend further along the positive or negative y-axis. The incoming parallel fibers are initiated with 12 phases similar to granule cells in the main volume of the simulation cube. At each phase, they are randomly placed in 2 areas of the extended cube (Figure 5). Their phase-by-phase distributions in z-axis follows the same allocations as the main granule cells. Their growth behavior is also the same as the parallel fibers described in the granule cell migration model section.

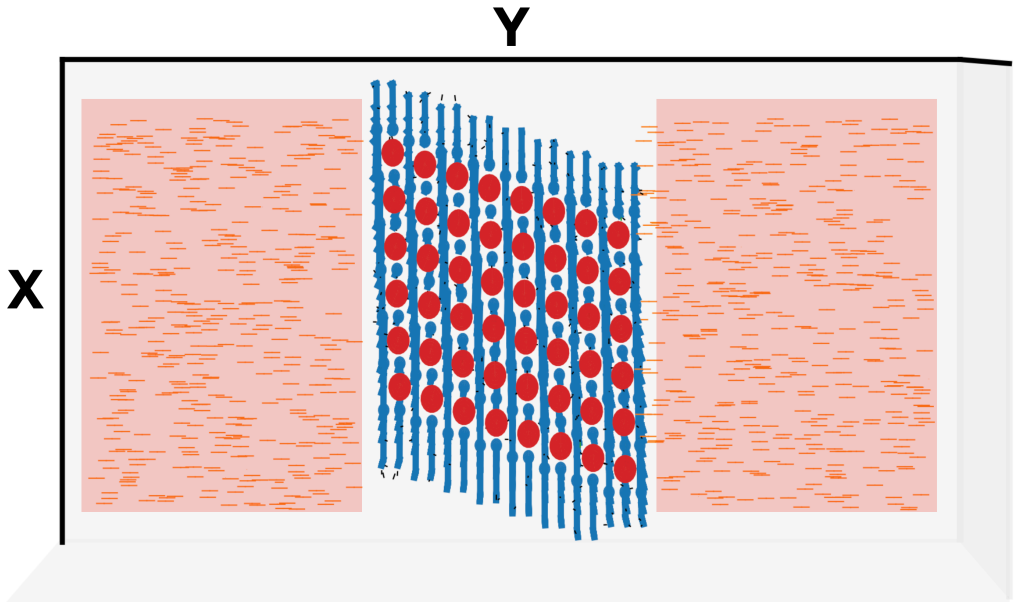

Figure 5. Extended granule cell model. Top view of the extended granule cell model right after initiations of granule cells and incoming parallel fibers (at cycle = 7). Large red spheres are Purkinje cell somas, and smaller blue spheres are somas of Bergmann glia with their processes. Color-shaded rectangles shows 2 areas where incoming parallel fibers are initiated. Thin orange cylinders in the shaded area are extending parallel fibers, and tiny black structures at main area (where Purkinje cell somas and Bergmann glia line up) are horizontally migrating granule cells.

2.4. Purkinje cell model

2.4.1. corresponding timeline and simplifications

The Purkinje cell growth in the model correspond to Purkinje cells in mouse in postnatal days (P) 4 to 10. Therefore, migrations of Purkinje cells and dendritic remodeling up to early stellate stages are not simulated by the model. The simulation starts from P4 of later stellate stage, meaning that there are newly formed dendrites on the upper sphere of the soma and retractions of dendrites in the bottom half have already occurred. The radius of dendritic fronts is much smaller than real dendrites (0.05 μm) assuming the dendritic leading processes are elastic (personal communication, Prof. Kengaku and Prof. Fujishima), and they will grow ticker at the later developmental stages that are not simulated in the model Starting with P4 Purkinje cell somas, their dendrite formation and retraction are simulated.

The initiation of dendritic growths waits during granule cell migrations of phases 1 to 5, and starts only at cycle 65 with phase 6 granule cell migrations. 10-20 simulations (sampling size is extended in Scenario 2 and 3) of these first set of initiations plus 5 cycles of dendritic tree growths and phase 7 granule cell initiation were generated with different random seeds. These 10-20 simulations were used as the common initial conditions for the different growth and retraction scenarios. Simulations with the same random seeds in NeuroDevSim never produce exactly the same results, especially for crowded simulations like our model, due to unpredictable differences in timing of the parallel processing. In order to keep the initial conditions reproducible to every simulation, the 10-20 initial sets of the simulations were used, ensuring that every set of simulations has the same initial 70 cycles of simulation.

2.4.2. growth algorithms

2.4.2.1. root dendrites

At the initiation of Purkinje cell dendrites, each soma grows 5 root fronts from its upper half sphere. Each root front is 7.5 μm in length and extends towards random directions, but separated minimally 2 μm and maximum 4 μm in the y-axis. Upward force in z-axis is also added to the random growth directions reflecting a phenomenological effect of the external granule layer whose presence is required for upward growth of stem dendrites (Altman, 1976).

2.4.2.2. elongate to heading plus upward

When there is no free parallel fiber fronts available within 5 μm around the tip of a dendrite front, the dendrites continue growth along the direction of their current heading with a small upward force. This upward force assumes phenomenological involvement of interneurons in the molecular layers, basket cells and stellate cells, as they are in the living system (Altman, 1976). However, molecular interneurons were not physically present in this model. The default growth step is 5 μm with a few exceptions when it is

reduced to half. One is when a dendritic tree is not branched yet and the other is when no synaptic target is detected. In order to secure a stem dendrite proximal to soma, the growth of the dendrite is restricted to upward and only considers dendritic repulsion (see dendrite-dendrite repulsions subsection) when branch order is 0. As a counter measure to avoid no branching at the bottom layer of trees, growth step is reduced to half which increases the chance to hit the random branching probability (see branching subsection). A growth step is also reduced to half of the default while no target is detected in order to having more chance to explore the current layer. This behavior refers to overelaboration of dendritic tree upon sparse over expression of GluD2 which takes role in synaptic communications between the dendrites and parallel fibers, and synapse formation can be a signal to stop the exploration (Takeo et al., 2021). In the model, dendrites stop growing when they hit z = 100 as it considered to be beyond the simulated development phase (P4 to P10).

2.4.2.3. dendrite-dendrite repulsions

Repulsions with the closest dendritic tree fronts of other cells or of the same cell are implemented in the model. Strength of the repulsion force is given by a repulsion factor = 0.6 divided by a distance in y-axis between a growing dendrite front and a closest dendrite front. If the repulsion force resulted in more than a given repulsion limit of 1.0, the repulsion force is re-assigned as 1 μm growing away from the closest dendritic fronts.

2.4.2.4. grow towards and perpendicular to available parallel fiber fronts

The model assumes that the dendrites grow towards their future synaptic partner parallel fibers, and reflects dendrites' preference of perpendicular growths to parallel fibers observed in biological systems (Nagata, Ono, Kawana, & Kimura-Kuroda, 2006). In the model, a tip of the dendrite front grows towards a nearby (within 5 μm range) synapse free parallel fiber front. When a tip of the growing dendritic front is close enough to the free parallel fiber front surface, it makes a synapse and the dendritic front grows a new front to a point on a plane perpendicular to the parallel fiber. The close enough distance for making a synapse is 1.0 μm from the center of the dendrite and parallel fiber fronts which are 0.05 μm and 0.1 μm in radius respectively.

2.4.2.5. branching

Branching of Purkinje cell dendrites occurs at its tips as observed in living systems. Two branching patterns were implemented in the model: random branching and directed branching. In both cases, new branching events are forbidden for the next 2 cycles for descendants of the branched fronts.

Random branching

For random branching, branching rate is quite small ($p < 0.08$ per simulation cycle; one simulation cycle is about 1 hour) referring to branch rates in vitro (0.26 times / 3 hrs, (Fujishima et al., 2012)). The first branch extends to a heading direction of the tip front plus small random factors (mean = 0, width = 1.0, max_angle = 20). The second branch extends on the same x-z plane, but separated by random degree (mean = 65, sd = 20,

normal distribution) from the first branch. Physical presence and synaptic interactions of climbing fibers are not introduced in the model. Deprivation of climbing fibers caused reduced branching patterns of Purkinje cell dendritic trees in vivo (C Sotelo & Arsenio-Nunes, 1976). However, the model is not intended to simulate the consequence of climbing fiber absence and effects of physical and synaptic absence of climbing fibers is disregarded.

Directed branching

When a direction towards a target parallel fiber front is far from the current growth heading of a dendrite front, the tip dendritic front attempts directed branching. The first branch extends closer or perpendicular to the target parallel fiber fronts depending on how they close to each other. The second branch is sampled from random point from the heading direction (mean = 0, width = 1.0, max_angle = 20) with some upward force depending on inclination of the tip front in y-axis. If the tilt in y-direction is stronger than dendritic repulsion limit (= 1.0 μm), strong upward force is given to correct the growth directions.

2.4.2.6. Collisions

When Purkinje cell dendritic fronts experience collisions, the code use the built-in solve_collision() method, as described in the granule cell migration model section, to find a detour to reach a destined position. If it fails, the front tries another solve_collision() in the next cycle as its last attempt.

2.4.3. retraction algorithms

Three different retraction algorithms are implemented with the model; trigger dendritic retractions at fixed cycles, by maturation status or by relative network activity levels. Dendritic growth for all the cases starts at cycle 65, waiting for the molecular layer to be filled with parallel fibers of granule cells. Two phases of retraction are implemented in all scenarios: first 3 dendrites of the 5 are retracted and later the 2 remaining compete to become winners. This two-phased retraction scheme is inspired by unpublished statistical data of Purkinje cells from Prof. Yukari Takeo where the final dendritic selections in vivo usually turn out to be competitions between two relatively largest candidate trees.

The fixed timing scenario hypothesized that timings of dendritic retractions are controlled by an internal clock of Purkinje cells. In the model, the first and second phase retractions happen on assigned simulation cycles. At these fixed cycles, the winners are chosen by relative numbers of synapses per dendrite in each cell. A relevant set of cycles identified in the scenario 1 is used as benchmarks to start checking maturation and activity levels of dendritic trees in following two scenarios.

The second scenario initiates retractions by comparing 2 kinds of maturation levels; size of dendritic tree or number of synapses with parallel fibers. Maturation by tree size focuses on internal signals of growth, and surrounding structures are treated as physical

obstacles to develop the trees. Conversely, maturation by synapses focuses on intercellular communication, and defines a tree sophistication by number of synapses with granule cells. Comparing that all Purkinje cell start the retractions at the same cycles in the scenario 1, each cell experiences retractions in different cycles according to their maturation status in the scenario 2. Also, scenario 2 uses universal thresholds for maturation parameters while winner trees are chosen by relative numbers of synapses in scenario 1,

The third scenario, retractions by network activity, focuses on synaptic interactions with dendritic trees and granule cells as in maturation by synapses in scenario 2. Instead of simply counting synapses in scenario 2, varied values of signals are assigned with synapses depending on the firing activity of granule cells. Also, first retractions of the third scenario depend on relative signal transductions of dendritic trees on each cell while the maturation scenario has universal thresholds for every Purkinje cells.

2.4.3.1. Scenario 1: Fixed timing

The first scenario is controlled by changing combinations of 2 parameter sets: WholeCheck_cycle_1 and WholeCheck_cycle_2, both assign cycles of simulations. A first dendritic retraction initiates at WholeCheck_cycle_1, which causes immediate reactions of 3 out of 5 dendritic trees according to number of synapses on each tree. Then, the 2 trees with largest numbers of synapses at this cycle keep growing. At WholeCheck_cycle_2, each Purkinje cell selects a winner dendritic tree from the lasting two candidate trees by number of synapses. The one with largest numbers of synapses keeps growing as a winner tree and the other retracts immediately. The value range for WholeCheck_cycle_1 was 72 to 100 cycles, and that of WholeCheck_cycle_2 was 74 to 124. 25 different combinations of parameter sets were tested with 10 simulations each. Since retractions are determined by relative numbers of synapses, most Purkinje cells always ends with having at least one dendritic tree. In theory, a few Purkinje cells can have more than 2 primary trees if the number of synapses is exactly the same at given cycles, but this was not observed during the simulations.

2.4.3.2. Scenario 2: Dendritic maturation

Instead of letting a common internal clock automatically decide the retraction timing, universal maturation levels of dendritic trees control the timing of retractions. This dendritic maturation is defined by one of two factors: size of dendritic tree or number of synapses with parallel fibers.

By tree size

‘Size’ of a dendritic tree refers to number of dendrite fronts in the model. This is a reasonable measure for total dendrite size because lengths of dendrite fronts are relatively constant, except when not finding synaptic partner or solving collisions. Three parameters are compared in this scenario: Whole_1st (‘Whole’ refers to a whole cell), 1st_f_th (‘f’ for fronts and ‘th’ for threshold), and Whole_2nd. Whole_1st assigns a threshold for total fronts of a Purkinje cell to start the first retraction process, and 1st_f_th gives a threshold number of fronts for individual dendritic trees of a cell. At the first retraction stage,

dendritic trees that do not reach the 1st_f_th retract. Whole_2nd controls a total number of whole cell fronts to initiate the second retraction phase. In the second retraction stage, the dendritic tree with largest number of fronts is selected as a primary dendrite, and the rest of candidate trees retract. The value range of Whole_1st was from 200 to 600, that of 1st_f_th was 20 to 160, and Whole_2nd was 350 to 800. In total 59 different combinations of parameter sets were tested with 10 simulations each and later some of them extended to 20 simulations.

By number of synapses

For deciding the maturation by synapses, universal thresholds for number of synapses is introduced rather than comparing relative numbers at given cycles in the fixed timing scenario. Three parameters are used in this scenario: Whole_syn_1st ('Whole' for a whole cell and 'syn' for synapses), 1st_s_th ('s' for synapses and 'th' for synapses), Whole_syn_2nd. Whole_syn_1st is a total number of synapses for each Purkinje cell to initiate the first retraction process, and as in by tree size case, dendritic trees who reached the first synapse number threshold, 1st_s_th, keep growing while others retract. Then, when a cell reached a second whole synapse number threshold, Whole_syn_2nd, all remaining dendritic threes retract other than a tree with largest number of synapses. The value range of Whole_syn_1st was from 60 to 110, that of 1st_s_th was 5 to 40, and Whole_Syn_2nd was 120 to 260. In total 97 different combinations of parameter sets were tested with 10 simulations each and later extended with 20 simulations.

For the 2 maturation cases in the scenario 2, retraction events for each Purkinje cell happen at different timing, which is closer to the real developmental scenario. Also, compared to Purkinje cells having just two candidate trees after the first retraction phase in scenario 1, Purkinje cells can still have more than 2 dendritic trees after the first retraction stage because of high number of fronts or synapses than given thresholds. On the contrary, retraction events do not happen if values for the thresholds are too high and Purkinje cells cannot reach the high threshold by the end of simulation cycles (up to 220 if any active front exist). As possible in scenario 1, Purkinje cells can have multiple primary trees if more than 2 trees have the exactly the same numbers of fronts or synapses at the second retraction process.

2.4.3.3. Scenario 3: Network activity

The third scenario implements differences in synaptic activity in dendritic trees due to varying firing rates of granule cells. A synapse from a parallel fiber front has a synaptic input that scales with the average firing rate (arbitrary unit in range 0-10) of the afferent granule cell. The synaptic signal is calculated as an integration of synaptic input with a decay of 20.0: signal = signal + synaptic input - (signal / decay). These signals are locally summated for each dendritic tree at later simulation cycles. Maximum firing rate changes according to the migration status of granule cells. Maximum firing rate = 0.2 is assigned when granule cells are still migrating, and it is updated to new maximum firing rate = 10.0 when granule cells arrived at the internal granular layer. Incoming parallel fibers from outside of the main volume of the simulation cube already have the new maximum

firing rate = 10.0 assuming that their granule cells already reached to the internal granule layer. Minimum firing rate is always 0. Value of firing rate is given by multiplying a random number from the uniform distribution with maximum firing rate when a granule cell extends its axon and then with new maximum firing rate when arrives at the internal granular layer.

The scenario 3 is controlled by two parameters: Whole_signal_1st and Whole_signal_2nd. Whole_signal_1st tests total signal summed over all Purkinje cell dendrites to start the first retraction phase. Once a cell reaches Whole_signal_1st, it calculates mean value of the signal by dividing the total by number of dendritic trees. Dendritic trees with more signal than the mean keep growing and other ones retract. Whole_signal_2nd assigns a total signal for a Purkinje cell to initiate the second retraction phase. At the second phase, the dendritic tree(s) that has the highest value of summed signals is chosen as a primary tree by retracting others. The value range for Whole_signal_1st was 10,000 to 15,000, and that of Whole_signal_2nd was 13,000 to 20,000. 11 different combinations of parameter sets were tested with 10 simulations each, and later extended with 20 simulations for three parameter combinations which earned the largest average numbers of synapses. Dendritic trees that got no synapses but stayed until the end of simulation because the corresponding Purkinje cell could not hit the threshold were excluded from analysis. In this scenario, timings of retraction events are different for each Purkinje cell as in scenario 2. However, compared to the universal threshold for each tree to survive the first retraction given in scenario 2, the first retraction for the scenario 3 uses mean signal value. Therefore, each Purkinje cell has a unique threshold for the first selection process. Because this first retractions are decided by the mean, at least one and max 4 dendritic trees, if all 5 are successfully growing, stays up to the second retraction stage. An exception is that all trees of a cell have the exactly the same value of integrated signal, which results in retractions of all dendritic trees at the first retraction stage. Likewise, Purkinje cells can end up with having more than 2 primary trees after the second selection phase in the unlikely event that all the dendritic trees would receive identical synaptic input. Comparison of all 3 scenarios is shown in Table 1.

Table 1. Comparisons of the three retraction scenarios. The table summarize the differences between retraction scenario 1 to 3 mentioned in the main text. The right most column shows the actual number of resulting primary trees for each Purkinje cell used for analysis (240 simulations in Scenario 1, 940 in Scenario 2 (By Fronts), 1390 in Scenario 2 (By Synapses), and 715 in Scenario 3). In Scenario 2 and 3, '>2' is in parentheses because these are the cells that could not reach the second threshold defined by the parameters at the end of the simulation. In Scenario 3, 'Two' is also in a parenthesis because it is highly likely due to failing to reach the second threshold.

	Number of parameters	Retraction timing for each cell	1st retraction rule	2nd retraction rule	Possible numbers of primary trees after the 1st retraction	Actual numbers of total primary trees after the 2nd retraction
Scenario 1	2	The same	Relative threshold	Relative threshold	2	Zero: 0 One:5629 Two: 131
Scenario 2 (by Front)	3	Different	Solid threshold	Relative threshold	0 - 5	Zero: 875 One: 21482 Two: 120 (>2: 83)
Scenario 2 (by Synapse)	3	Different	Solid threshold	Relative threshold	0 - 5	Zero: 67 One: 32873 Two: 375 (>2: 45)
Scenario 3	2	Different	Relative threshold	Relative threshold	0 - 4	Zero: 0 One: 17130 (Two: 24) (>2: 6)

2.4.4. Purkinje cell growth without synaptic or physical interactions with granule cells

2.4.4.1. Scenario S0A: randomly selecting one dendritic tree

In this scenario, Purkinje cells skip the dendritic selection stage. Although dendritic trees are growing surrounded by granule cells, they are not involved in the selection. Instead, a single primary tree was randomly selected for each Purkinje cell 7 cycles after initiating growth of 5 candidate trees. Therefore, only physical interactions of granule cells have influence on morphology of the winner trees. This scenario explores the importance of having a dendritic selection stage.

2.4.4.2. Scenario S0B: grow all the dendritic trees and no retraction

This scenario never triggered retractions of candidate trees, and provide physically more competitive environment for space availability. This case does not use synaptic interactions with granule cells, but physical obstructions by granule cell structures can affect dendritic tree morphology as in scenario 0A. This scenario also questions the dendritic selection stage by keeping growth of all the candidate trees, and makes use of all the growing options.

2.4.4.3. Scenario S0C: growing without granule cell environment and retraction triggered by tree size

Purkinje cells in Scenario 0C grows in the simulation cube without granule cell migration. Therefore, only Bergmann glia and surrounding Purkinje cells will cause physical interference. The retraction mechanism for this scenario recruited the best parameter set in scenario 2 by tree size so that they can initiate retractions without granule cells. Difference between Scenario 2 by tree size and Scenario 0C is that the former considers physical interactions with granule cells, which is absent for the latter. This scenario shows Purkinje cell morphology given by behavior of the intrinsic growth algorithm implemented in the model. Note that, above Scenario 0A and 0B use the common 10 initial conditions as in Scenario 1 to 3, but Scenario 0C did not use these prepared databases as the scenario does not simulate granule cells. Scenarios S0A and S0B had 10 simulation samples each, but only 5 samples could be collected for scenario S0C due to lack of time.

2.5 Data analysis

2.5.1 Analysis of granule cell migrations

For analyzing the granule cell model, success rates of radial soma migrations, formation of a T-junction, and extensions of parallel fibers were assessed (Figure 6). The data is extracted from the SQL database file using a python script. The success rate for radial soma migration counts cells that completed transfer of their somas below $z = 4$ μm. At $z = 4$ μm is the top of the Purkinje cell layer ($-11 < z < 4$ μm) in the simulation cube. Since we focus on constructing environment of the molecular layer ($z > 7$μm), this easy criterium for radial migration completion is used. The success rate for formations of a T-junction counts cells which could extend an axon and two parallel fibers from the axon. T-junctions refers to a structure composed of an axon as a vertical stem and two parallel fibers extending horizontally from the top of an axon making a “T” shape. A failure in forming the T-junction means an axon of a granule cell soma could not extend any parallel fibers or could extend only a single parallel fiber. The success parallel fibers are those that reached the y-edge of the simulation cube. A goal y-position of parallel fibers growing forward (towards positive y direction) is:

(max y-value of the cube) - (growth step of a parallel fiber)

and that of growing backwards (towards negative y direction) is:

(minimum y-value of the cube) - (- growth step of a parallel fiber).

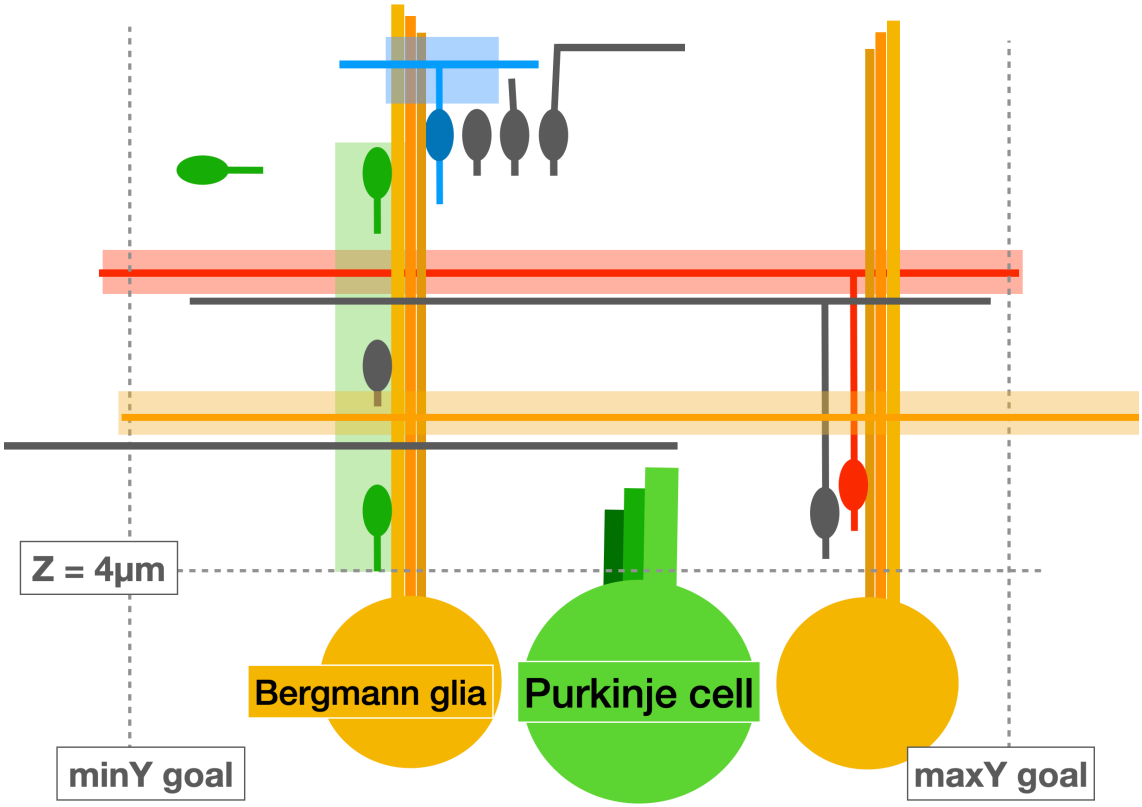

Figure 6. Criteria for Success. Red granule cells on green shade shows start and end point of radial migration. If granule cells stuck in between like the grey cell, they are not counted as success. The green granule cell on the end position of radial migration succeeded its radial migration, but it is also an example of failing in extending an axon. Blue granule cell axon with a blue shade shows successful formation of a T-junction. Grey ones next by it are examples of failed T-junctions. Red parallel fiber on a red shade shows a successful parallel fiber growing from the main simulation volume, while the grey one below which got stuck before reaching y-axis goal is not counted as success. Yellow parallel fibers in-growing from the outside of the main volume is a successful incoming parallel fibers fully extended in the main volume, and grey one below is a failed incoming parallel fiber.

2.5.2 Analysis of Purkinje cell primary dendrites

In order to avoid edge effects, 24 Purkinje cells enclosed by outer Purkinje cells are sampled for analysis (shaded Purkinje cells in Figure 7). For all scenarios, morphology of resulted dendritic trees are analyzed and compared according to the following criteria:

1. Number of Winner dendritic trees, counting final number of primary trees in each Purkinje cell.

2. Size of the winner trees, assessed by number of fronts and max path length (tip to the center of somas) of the primary trees. Number of fronts is further investigated in 3 area divided by z-axis (area 1: $z > 40$ μm, area 2: $40 \leq z < 80$ μm, area 3: 80 μm $\leq z$).

3. Number of synapses on the winner tree, counting number of synapses with parallel fibers of granule cells on a resulted primary dendrite.

4. Max y-distance of the winner tree, representing the flatness of a winner tree, and calculated by difference between max end y-position and minimum end y-position of dendritic fronts.

5. Max x-distance of the winner tree, representing width of the dendritic tree, and calculated by a difference between max and minimum end x-coordinates of a primary tree.

6. Number of branch points and terminal points, branch points are counted by number of a winner dendritic parent fronts with 2 front children and terminal points are those with no front child. Number of terminals should always be number of branch points plus one, because of geometrical rule for binary branching. Both criteria are further assessed by 3 areas divided in fixed z-axis as for number of fronts.

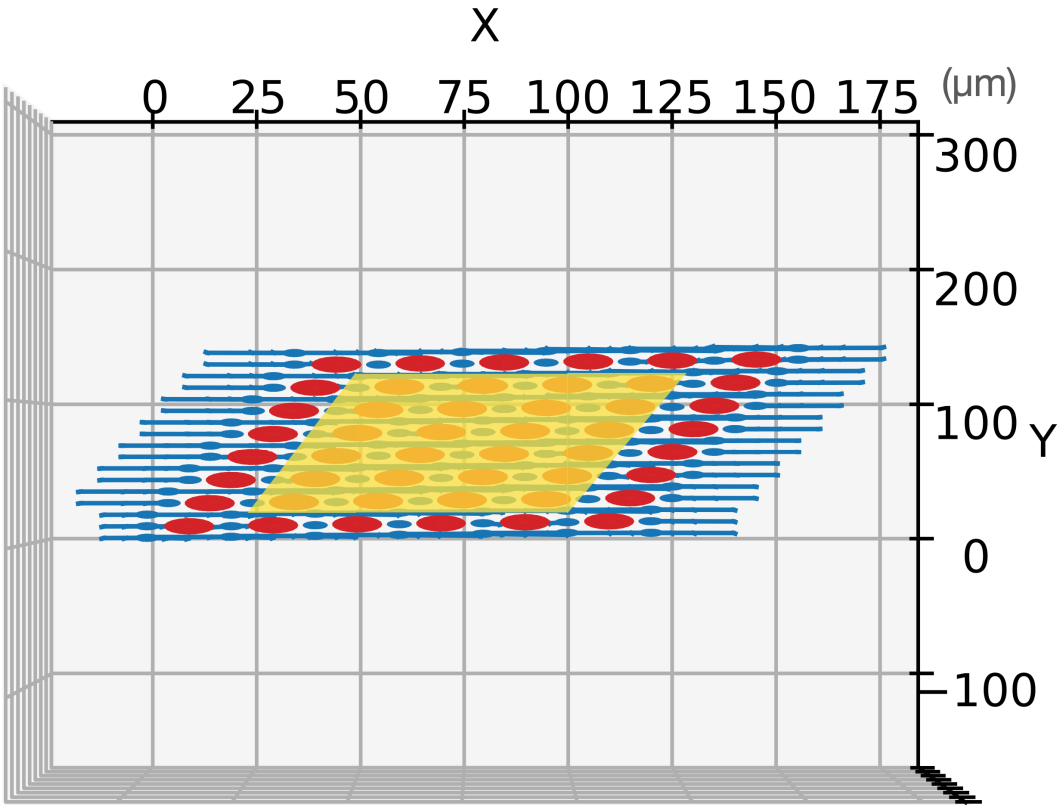

Figure 7. Purkinje cells to be analyzed. A simulation volume viewed from the top (x-y scale is not adjusted). Large red spheres are Purkinje cells somas, and smaller blue spheres with extended processes are Bergmann glia. Purkinje cell somas shaded by yellow area were analyzed.

3. Results

3.1 Results from the granule cell migration model

The granule cell model represents the environment for dendrite growth of Purkinje cells and consists of 3024 granule cells, 118 Bergmann glia, and 48 somas of Purkinje cells. As mentioned in the Methods section, dendritic growth of Purkinje cells is not implemented in this model. A simplified code structure for managing granule cell migrations is shown in Figure 8 (see Table 2 and Table 3 for brief descriptions about terms and methods in Figure 8). What the whole simulation cube looks like after the migration completed is shown in Figure 9.

```
Class Granule Cell

def manage_front():
  if soma:
    self.gc_soma()
  elif leading process:
    if mode == 1:
      self.extend_to_BG()
    elif mode == 2 or 3:
      if distance_to_BG < close_enough:
        self.extend_down()
      else:
        self.extend_to_BG()
    elif mode == 4:
      self.arrived_at_bottom()
    else (mode == 5 or -1):
      self.disable()

  elif axon and initiated axon:
    self.axon_branch()
  else (parallel fibers):
    self.pf_extension
```

```
def gc_soma():
  if mode == -1:
    self.retract()
  if mode == 2 and not yet extend an axon:
    self.rootaxon_initiation()
  if having a leading process:
    if have a grand child:
      if have an axon:
        self.migrate_soma(trailing_axon=True)
      else (only leading process):
        self.migrate_soma()
    else:
      return (wait)
  elif mode == 0:
    self.find_target_BG()
  elif mode == 1:
    self.extend_to_BG()
  elif mode == 2 or 3:
    self.extend_down()
  elif mode == 4:
    self.arrived_at_bottom()
  else (mode == -1 or 5):
    self.disable()
```

Figure 8. Simplified code structure for modeling granule cell behaviors. Simplified version of granule cell code only showing manage_front() and gc_soma() methods. All fronts generated in the simulation first call the manage_front method, and call another method depending on which structure of front they are (e.g. soma, leading process, etc.) and on their migration status. When a front is soma, it calls gc_soma(). In the gc_soma(), the code controls the behavior of the soma according to the status (modes) of the soma. Code shown has been modified to make it easier to comprehend.

Table 2. Description of each mode status in the granule cell model. This table briefly describes the conditions for each mode of granule cells appearing in Figure 8.

migration modes for granule cells	
mode 0	initiated and search for nearby Bergmann glia target
mode 1	found the target and migrate horizontally
mode 2	got close enough to the target Bergmann glia, starts migrating radially along the glial process
mode 3	extended a descending axon during the radial migration
mode 4	left the glial process and keep migrating downwards
mode 5	reached a destined z-area and stop the migration
mode -1	faced unsolvable collisions with surrounds and removes itself from the simulation volume

Table 3. Descriptions of each method in granule cell model. This table explains roles of each method called in Figure 8.

methods for the granule cell migrations		
manage_front()	for all fronts	initial method that every active front calls at each cycle
gc_soma()	for somas	manage operations of each soma
find_target_BG()	for somas	search for nearby Bergmann glia and define the closest one as its target
extend_to_BG()	for somas and leading processes	horizontally grow a leading process towards the glial target
extend_down()	for somas and leading processes	radially grow a leading process downwards
rootaxon_initiation()	for somas	extend an axonal front from a soma opposite side to its leading process front
axon_branch()	for axons	extend two parallel fiber fronts from an initial axon
pf_extension()	for parallel fibers	grow parallel fibers in horizontal directions
arrived_at_bottom()	for somas and leading processes	reached the bottom of the molecular layer; grow further down or stop growing if reached the internal granular layer
migrate_soma()	for somas	a build-in method of NeuroDevSim: migrate a soma to the position of a connected leading process front. If setting trailing_axon parameter True, the current location of the soma is replaced by a trailing axon front

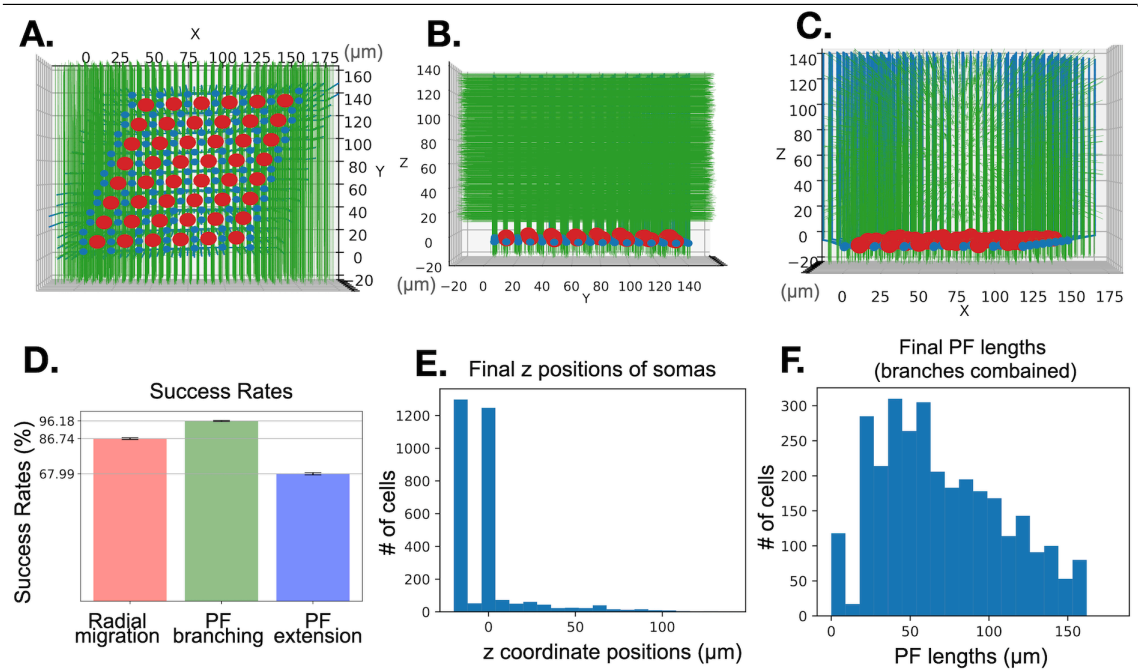

Figure 9. Results from the representative granule cell model. A,B,C: A final simulation cube of an example case visualized from 3 directions: a top view is shown on the left, and side views on the right. Red large spheres are Purkinje cell somas. Blue small spheres with processes growing upward are Bergmann glia. Numerous green thin threads are axons of granule cells. D. 3 histograms showing variations from 10 simulation samplings from the granule cell model. Red histogram for success rate of total parallel fiber extensions, green is for success rate of radial migrations, and blue for parallel fiber branching to form T-junctions. Error bars show standard deviations, and coefficient of variation values are 0.009, 0.005, and 0.003 respectively. E: A histogram showing final positions of granule cell soma on z-axis in the representative case. F: A histogram showing final lengths of the parallel fibers in the representative case.

3.1.1. Statistics of an example case

Success rates of a representative granule cell model for the following migration processes were analyzed: radial migrations, formations of T-junctions, and parallel fiber extensions. Variations of 10 simulation samples are also shown in Figure 8.

Radial migrations: 2597 granule cells reached the internal granule layer (z <= 4) out of 3024 cells, so 85.88% of the descending cells succeeded in the radial migration.

T-junctions: 2900 out of 3024 cells made a root axon and two parallel fiber fronts, so 95.90% of each root axon extended two parallel fiber segments.

Parallel fibers: 2022 out of 2915 fibers reached front (y <= -16) and 1906 out of 2914 reached back (y >= 156), in total 67.39% of parallel fibers extended through the complete volume. Because these fibers originate from T junctions inside the volume, all are expected to reach both ends for an expected length of 2034 ± 622μm in 2.5-month-old mice (Huang, Wang, & Huang, 2006). For 300-400g rats, it is 4.2-4.7 mm (Pichitpornchai, Rawson, & Rees, 1994).

Biological measurements of the granule cell density in the cerebellar cortex range from 500,000 to 6,562,500 cells per mm^3 cube (Zanjani et al. (1997) and Steen (2006) are compared in Keller et al. (2018)). With the studies showing the ratio of Purkinje cell and granule cell populations, there are 132 (Sturrock, 1989), 171 (Vogel, Sunter, & Herrup, 1989), 274 (Harvey & Napper, 1988), or 778 (Lange, 1975) granule cells per single Purkinje cell. We have 48 Purkinje cells in the model, so there should be 6336, 8208, 13152, or 37344 granule cells in an adult mouse. We simulate the mouse cerebellar cortex up to postnatal day 10 and granule cells keep proliferating until around postnatal days 30. Although it is difficult to draw conclusive population numbers of granule cells, the model generates many more granule cells than Purkinje cells during the target developmental stage in the simulation. However, it still difficult to achieve 100% success rate of radial migrations of granule cells with the current density of granule cells in the model. In biological systems, failure of radial migration is rarely observed (personal communication, Dr. Kengaku and Dr. Fujishima). Since the model is built to represent the molecular layer as an environment for Purkinje cells' dendritic tree development, the success line for the radial migration is set to the upper line of Purkinje cell layer. If checking final z-axis positions of granule cell migrations (Figure 9D), we can expect that it is even more difficult for granule cells to migrate through Purkinje cell layer filled with large somas. Similarly, extension of parallel fibers face the difficulty to manage crowded environment in the molecular layer. So far, no data available for failure rate of parallel fiber extensions to compare with are available, though more numbers of parallel fibers are expected in the real system for the proposed populations of granule cells. Although more than 60% of parallel fibers fully extended within the main volume of the simulation, many ended up with shorter lengths (Figure 9E). This model does not completely represent the real system, but is a fair first attempt enough to show the challenges of granule cell migrations.

3.1.2. Aborted cases

Although most of the cells could complete the soma migration and axon extensions, some cells could not accomplish intended migrations or extensions. At the Radial migration phase, 14.12% of granule cells (427 cells) could not reach the internal granule layer (z = 4). In the molecular layer, there is competition for limited space around Bergmann glia process which are wrapped by descending axons of early granule cells (Figure 10A). In addition to the blockage by granule cell axons, some of the cells did not succeed to get around parallel fibers running close by Bergmann glia processes (Figure 10B-1). At the end of the radial migration, granule cells also need to dodge the horizontally oriented root processes of Bergmann glia and then circumvent between large somas of Bergmann glia and Purkinje cells in the Purkinje cell layer (Figure 10C). Relatively few cells failed to

form T-junctions. 4.1% (124 cells) could not initiate their first descending axons, and 0.4% (22 cells) could not extend either or both initial parallel fiber fronts. Their extensions were interfered by descending axons or parallel fibers of other granule cells. For the Parallel fiber extensions, 32.61% (1901 fibers) of parallel fibers could not reach to the edges of the simulation cube. Their extensions were interfered by BG processes, descending axons surrounding the processes, and other parallel fibers who wiggled to evade obstructions (Figure 10D).

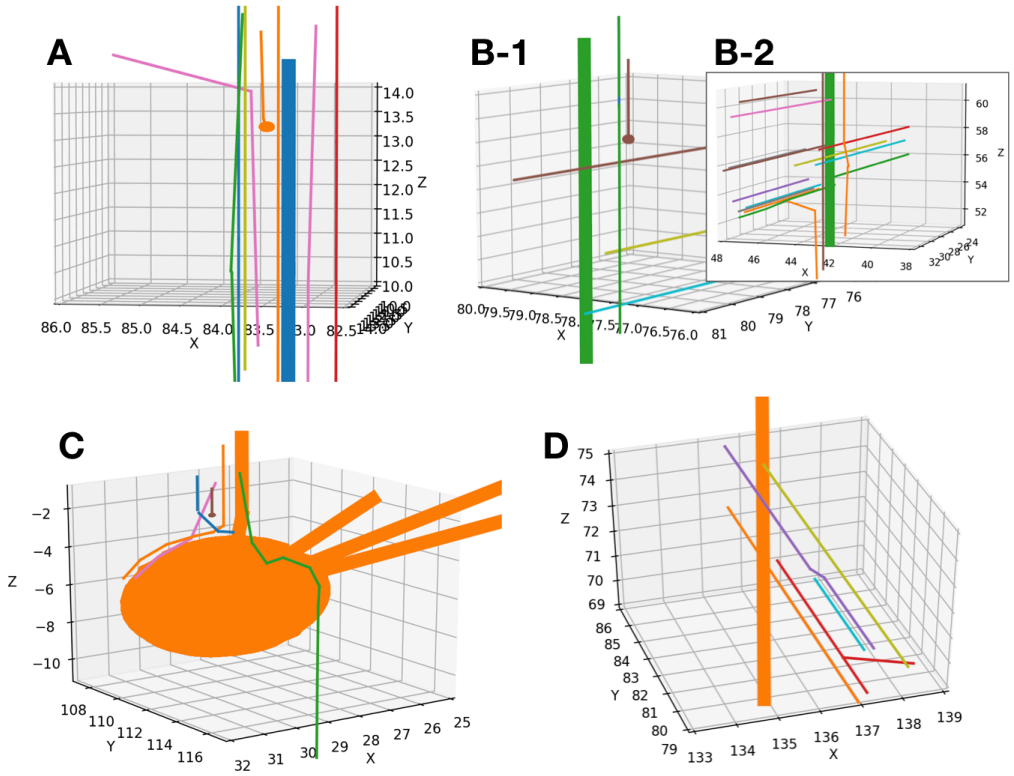

Figure 10. Example cases for granule cells that got stuck during migration or extensions. (A) A granule cell soma (orange small sphere) could not migrate further down as it was blocked by descending axons of other granule cells wrapping around a Bergmann process (blue thick cylinder). (B-1) A migratory path of a granule cell soma (brown small sphere) is blocked by a parallel fiber of another granule cell (horizontally oriented brown fiber). (B-2) a descending axon of successful granule cell (radially oriented orange fiber on the right side of a thick green Bergmann glia process) that could manage a similar situation as in B-1. (C) A granule cell soma (purple sphere) could not get around Bergmann glia soma (large orange sphere). Orange, blue, pink and green axons are from other granules that did manage to circumvent the spherical soma. (D) A parallel fiber (light blue) growing towards positive y-direction is interfered by another parallel fiber (purple) who grows to the opposite direction and wiggled to avoid a collision with the light blue parallel fiber. For the visualization, front radii are magnified to 10 times of the original radius. Granule cell somas are represented as spheres only for the figures. They are actually cylindrical fronts with same radius as their leading processes and descending axons in the simulation. Figure A was generated from a database named Note24_2d.db at cycle 44 out of 220 simulation cycles. B-1, B-2, and D are from Note24_3d.db at cycle 80/209. C is from Note24_3.db at 155/209.

3.2. Results from the extended granule cell migration model

The extended granule cell model additionally represents numerous parallel fibers traveling from distant part of the cerebellar cortex. The main volume (x1, y1, z1), (x2, y2, z2) = (-20, -20, -20), (180, 160, 140) μm^3 consists of the same amount of granule cells, Bergmann glia, and somas of Purkinje cells. At the extended y-axis volume (x1, y1, z1), (x2, y2, z2) = (-20, -20 —> -160, -20), (180, 160 —> 300, 140) μm^3, parallel fibers of 10296 granule cells join the interactions happening in the main volume. Figure 11(A-C) shows the model at the final simulation cycle. This model is constructed to include parallel fibers incoming from outside of the main volume as parallel fibers in 2.5-month-old mice extend to about 2 mm (Huang et al., 2006) which is roughly 11 times more than the length the 3024 granule cells' parallel fibers are expected to reach in the main volume of the model.

3.2.1. Statistics of a representative case

Radial migrations: 2437 granule cells reached the internal granule layer (z <= 4), so 80.59% of the cells succeeded in the radial migration. Therefore, less granule cells could complete the migration compared to the original model.

T-junctions: 2882 both branches, 95.30% of the cells successfully formed T-junctions.

Parallel fibers: 2033 out of 2918 fibers reached front (y <= -16) and 1915 out of 2911 reached back (y >= 156), in total 67.73% of parallel fibers extended through the complete volume.

Ingrowing parallel fibers: 2969 out of 10128 ingrowing fibers fully extended forward/back in the main volume, so 29.31% of parallel fibers growing from the outside of the main volume completed extensions through the volume.

Total parallel Fibers in the main volume: 3487 towards front and 3430 to backwards.

Variations of the success rates from 10 simulation samples are shown in Figure 11D. Success rates for radial migrations, T-junction formation, parallel fiber extensions of granule cells initiated in the original volume slightly decreased as the additional parallel fibers from the outside of the main volume became a new physical obstruction. Success rate of extension of ingrowing parallel fibers in the main volume is quite low. However, introduction of ingrowing parallel fiber still boosted the total number of fully extended parallel fibers in the main volume, from 3928 to 6669. The growth step size of parallel fibers is 4 μm and each front can form a single synapse with a Purkinje cell dendrite, so synaptic sites are minimally separated by 4 μm, except on shorter fronts made by solve_collisions(). Density of synaptic varicosity is 0.146 ± 0.027 varicosity/μm on parallel fibers in 2.5-month mice (Huang et al. 2006). Another imaging study claimed that there is one presynaptic terminal per 4 μm of parallel fibers and descending axons on average (Tasic, Michele et al., 2010). One parallel fiber in the model can form more or similar numbers of synapses with Purkinje cells than/as biological ones. The ideal density

of the parallel fibers are 11 times more than the granule cell population in the main volume. Forcefully adding more incoming parallel fibers could cause further decrease in radial migration rate of granule cells. The model provides decent opportunities for Purkinje cell dendrites to form synapses with parallel fibers with crowding as a physical constraint. However, the current design of the model is not capable of simulating physical interactions with the real, gigantic number of parallel fibers.

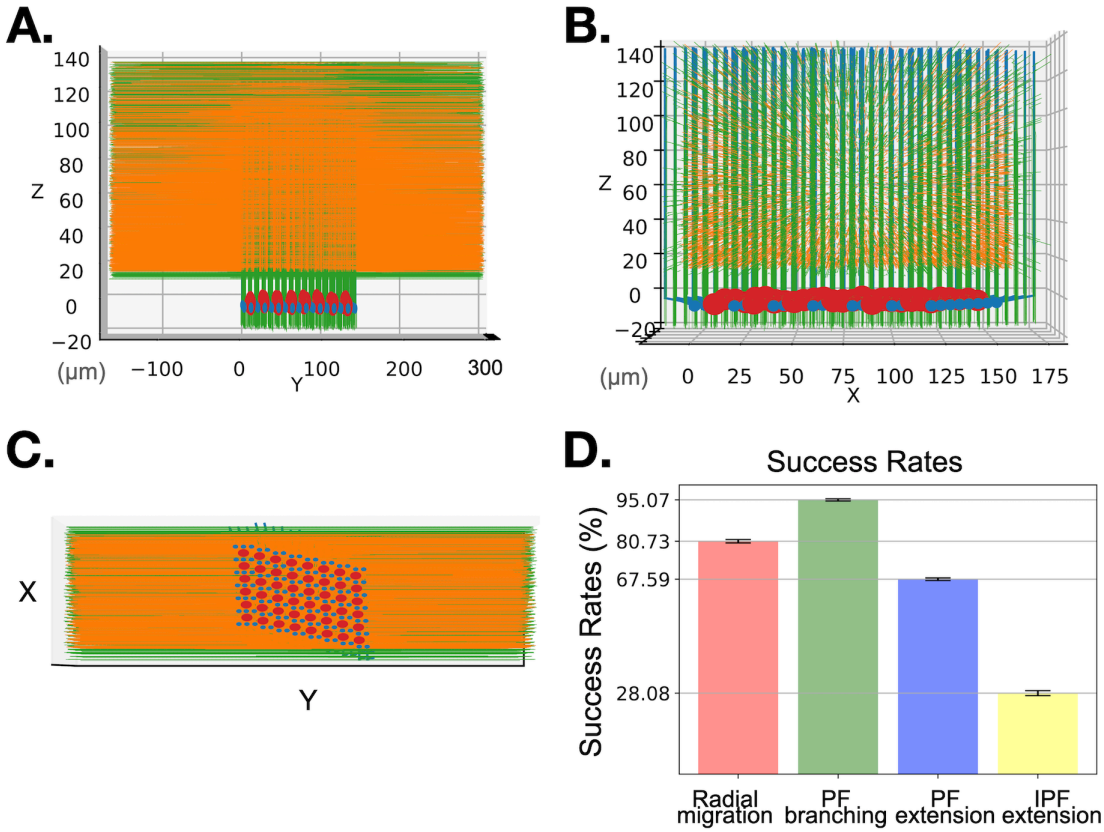

Figure 11. Extended granule cell model. A,B,C: A final simulation cube from the extended granule cell model is visualized from 3 directions: A and B are side views, and C is a top view. Red large spheres are Purkinje cell somas. Blue small spheres with processes growing upward are Bergmann glia. Numerous green thin threads are axons of granule cells in the main volume (where Purkinje cell somas and Bergmann glia are line up), and orange fibers are ingrowing parallel fibers. D: Bar plots show mean success rates from 10 simulation samplings from the extended model with error bars showing standard deviations. A red bar is for success rate of soma radial migrations, green is for success rate of parallel fiber branching to form T-junctions, blue for parallel fiber extensions initiated in the main volume, and yellow for parallel fibers growing from the outside of the main volume and fully extended in the main volume. Coefficient of variation values for each is 0.031, 0.007, and 0.007, and 0.004 respectively.

3.3. Results from Purkinje cell model

Three scenarios for distinctive growth environments and another three scenarios for different retraction strategies were simulated. Resulting winner trees of Purkinje cells were assessed based on number of synapses they generated for these different environments and retraction strategies. Comparisons of their morphology helps to understand the possible purposes of including a dendritic selection phase in the developmental course, considering the cost of limited resources and energy to grow and retract extra dendritic trees.

3.3.1. Results from 3 control growth scenarios

The goal of these 3 unique dendritic growth scenarios is to provide controls for scenarios that simulate specific retraction strategies (3.3.2). The control models specifically focus on investigating the influence of dendritic selection processes and physical presence of granule cells on dendritic tree morphology.

3.3.1.1. General characteristics of each scenario

Three different Purkinje cell growth scenarios were compared. Changes in dendritic path length over simulation cycles exemplify the resulting behavior of Purkinje cells in each of the 3 scenarios (Figure 12A, B, C). Simulations for Scenario 0A and 0B used the saved initial conditions, and initiation of dendrite growth starts at cycle 65. The 0A_growOne scenario randomly chooses a single dendritic tree out of five candidates at cycle 65 + 7 and retracts all others (visible at the beginning in each plot in Figure 12A). On the other hand, S0B_growAll scenario never initiates retractions and all the dendritic trees in each cell keep growing until they reached z = 100 μm (Figure 12B). S0C_noGC scenario did not use the saved database as there are no granule cells at all, and dendritic growth is initiated at cycle 5. After cycle 30, the simulation checks if cells grew more than 250 dendrite fronts in total. If a cell reached that threshold, front numbers are computed for each dendritic tree, and a first retraction occurs of trees that have less than 60 fronts. At cycle 30 + 7, a second check proceeds, choosing the tree with the largest number of fonts for cells having at least 400 fronts in total and retracting all other trees. In the example cells in Figure 12C, Purkinje cell 19 (PC_19) follow this two-phased retraction as dendritic trees are retracted in 2 different cycles. PC_15 and PC_24 retracted dendrites at a single cycle because all dendritic trees at the first screening phase were mature enough to have more than 60 fronts and retractions only initiated at the second phase.

A comparison of the average number of synapses with parallel fibers in winner trees shows differences between S0A, S0B, and S0C (Figure 12D). Most clearly, dendritic trees in S0C did not have any synapses because there are no granule cells. Each dendritic tree in S0A_growOne got a much larger number of synapses than S0B_growAll, probably since growing all candidate trees led to more intense competition over limited numbers of synapse locations with parallel fibers. Moreover, in S0B, more structures in the simulation cube can lead to a decrease in the number of fully extended parallel fibers, which makes the competition even more severe. As mentioned before, the granule cell

model has fewer parallel fibers than expected in the biological system. Although experimental data to compare number of synapses on dendritic trees at the age of interest is not available, it seems the model provided enough opportunity for dendrites to form synapses with parallel fibers. There is a correlation between max path length of a dendritic tree and number of synapses on a tree. Assuming that there are enough parallel fiber fronts to form synapses, the larger max path length in S0A than S0B contributed to the increase in number of synapses. Winner trees in S0C had an artificially much increased number of total fronts since smaller growth steps are used when no parallel fiber is detected in order to explore the space to find available synaptic partner nearby, resulting in (more) smaller fronts. Increase in total number of fronts can be also due to repetitively calling solve_collision() method to manage crowded environment.

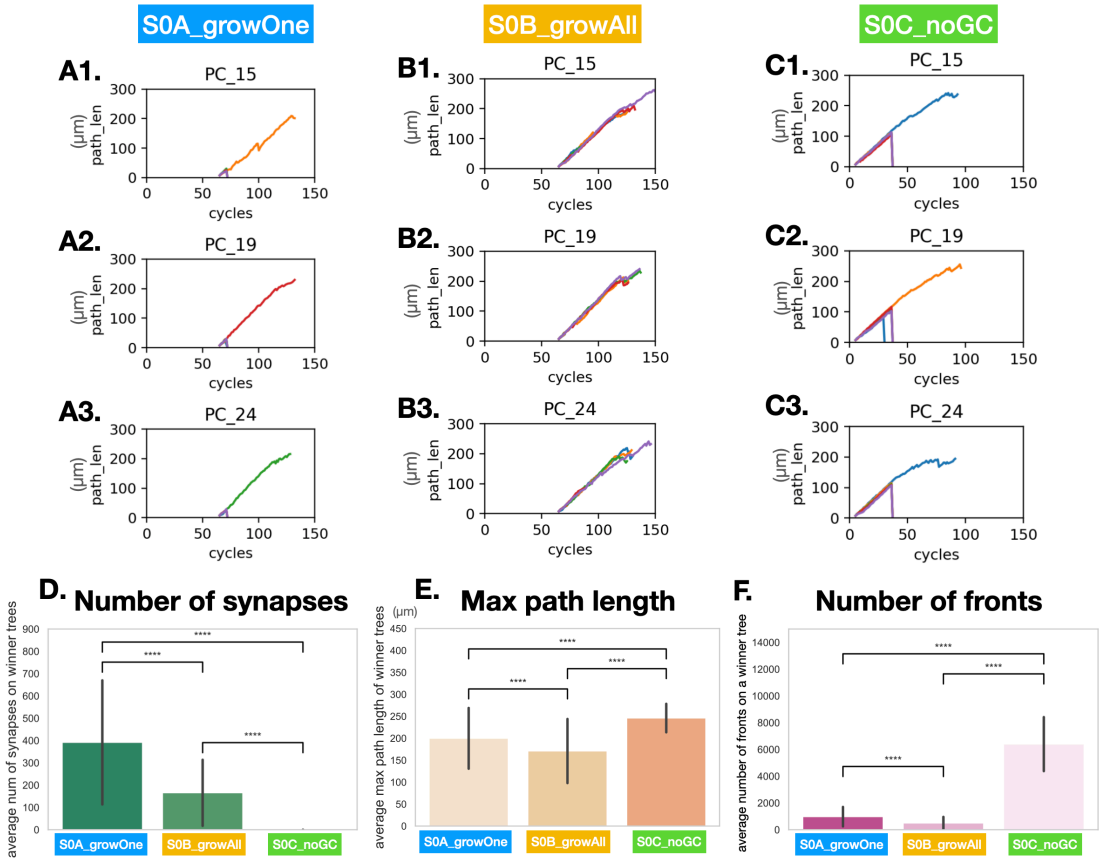

Figure 12. Characteristics of 3 growth scenarios. A1-3) The plots show change in max path length of each candidate tree at every cycle with a different line color for each dendrite. Three Purkinje cells were randomly selected from one of 10 simulations in scenario S0A growOne. B1-3) Similar plots as A1-3 from one of 10 simulations in scenario S0B growAll. C1-3) Similar plots as A1-3 and B1-3 from one of 7 simulations in scenario S0C noGC. D) Plotting the number of synapses on each dendritic tree in the three scenarios with error bars representing standard deviations. E) Plotting max length of each tree in the three scenarios with the error bars. F) Plotting number of fronts in each tree in the three scenarios with the error bars. P values: **** indicates $p < 0.00005$.

3.3.1.2. Y- and X-distance of winner trees

Characteristic morphology of the winner trees from these 3 scenarios was determined with further tree structure analysis (Figure 13). Especially, average max y-distance of the winner tree was greatly influenced by physical presence of granule cells (Figure 13A1, B1, C1, and E). This was due to a growth algorithm of dendritic tree which directs growth along a plane perpendicular to close by parallel fibers. The algorithm included dendrite-dendrite repulsions, which also contributed to flatness of the tree. But these repulsions have to be combined with physical presence of granule cells to establish distinct planar morphology as in S0A and S0B. Compared to the results from max y-distance, no remarkable difference in max x-distance was found at a glance (Figure 13A2, B2, C2, F). However, P values indicated significant differences between the data sets, and S0A and S0B has greater variation between samples compared with S0C. Physical hindrance from granule cells possibly contributed to extend the divergence in the tree morphology. Comparing the y-distance of S0A and S0B, S0A has slightly thinner trees than S0B. This was unexpected because competition over space availability in y-axis directions in S0B is more severe than S0A. In 150-180 postnatal day mouse, y-distance of dendritic trees in control mice was 13.9 ± 1.5 μm and x-distance was 82.9 ± 2.5 μm (Kim et al., 2011). Y-distance from scenario S0A and S0B are slightly thicker than the observed morphology, though Purkinje cell dendritic trees attains single planar morphology only after postnatal day 22 in mice (Kaneko et al., 2011) which is later in the development than simulated in the model (up to postnatal day 10). For growth in x-axis direction, the dendritic tree reaches its full x-width roughly by postnatal day 13 in mice (C Sotelo & Dusart, 2009). The x-distance of the 3 scenarios was marginally wider than that observed. Extended y-distance (28.7 ± 4.8 μm) and shrinkage of x-distance (40.0 ± 4.6 μm) was observed in reeler mice where the laminar structure of cerebellar cortex is lacking (Kim et al., 2011). S0C also got expanded y-distance compared to S0A and S02. However, results from S0C_noGC had much thicker morphology while keeping similar arbor size with S0A and S0B in x-axis.

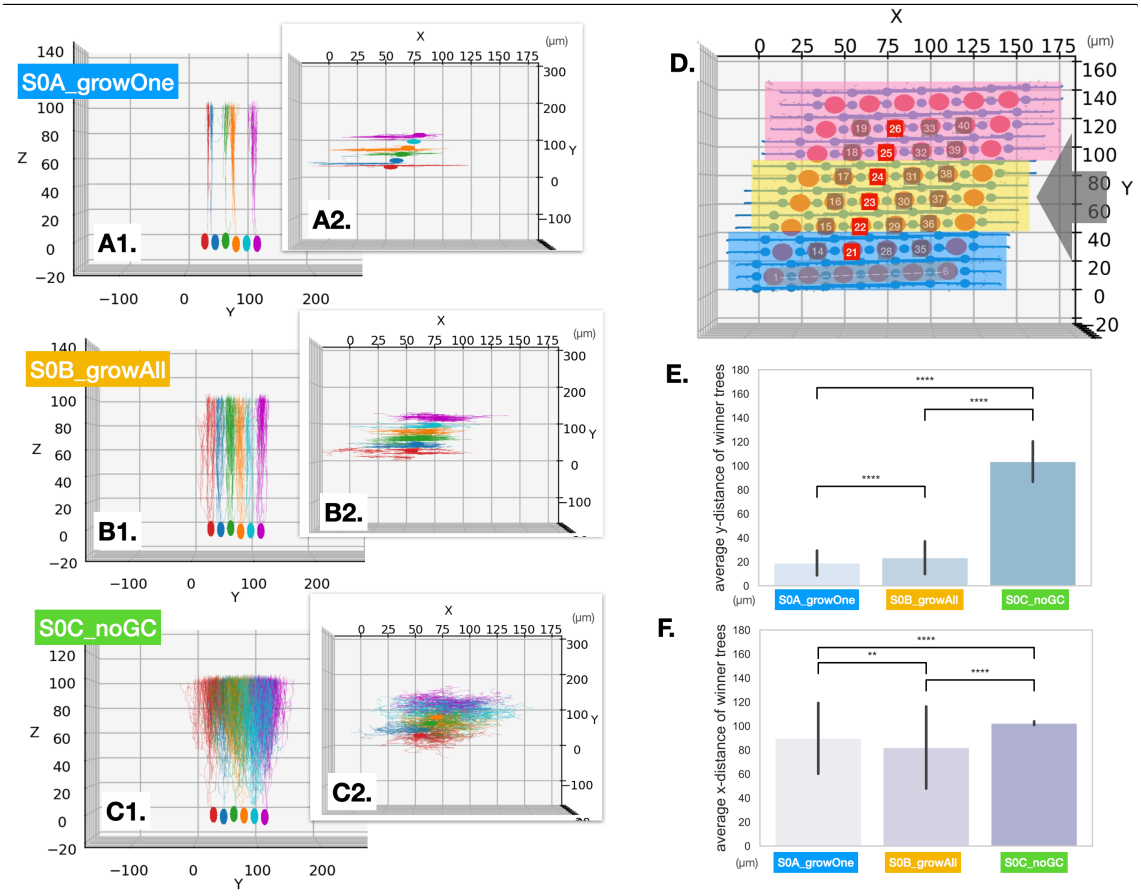

Figure 13. Arbor size of winner trees. A1) visualizations of Purkinje cells (pc_21 in red, pc_22 in blue, pc_23 in green, pc_24 in yellow, pc_25 in light blue, and pc_26 in magenta) from side view at cycle 120/220 for growth scenario S0A. Only selected Purkinje cells were visualized for convenience, while other structures (e.g. granule cells, Bergmann glia, and other Purkinje cells) are not shown. A2) A top view of A1. B1) A similar plot for scenario S0B. B2) A top view of B1. C1) A similar plot for scenario S0C. C2) A top view of C1. D) Top view of the original granule cell model to show the map of Purkinje cells visualized in A-C. The grey arrow indicates the viewpoints for A1, B1, and C1. E) Plots for comparing average max y-distance of each tree from the three scenarios with error bars indicating standard deviations. F) Plots for average max x-distance for the three scenarios with error bars. P values: **** indicates $p < 0.00005$ and ** is $p < 0.005$.

3.3.1.3. Winner tree morphology in 3 different z-axis area

In addition to the tree size in x- and y-axis, dendritic morphology was further analyzed and compared by dividing the structure into 3 areas in z-axis (Figure 14). In general, winner dendritic trees in S0C have much larger numbers of fronts, branch points and terminals at middle and distal area of the tree. Also, winner trees in S0A and S0C has largest number of fronts, branch points, and terminals as it goes to the distal area of the

dendrites. number of terminals in S0B has the same trend, but its number of fronts and of branch points are stable in the middle and distal area. In postnatal day 10 mice, the observed trend of dendrite length and branch points for different z-areas was quite flat (Takeo et al., 2021) (Figure 14H). In the model scenario, proximal area has less elaboration of the tree due to restricted growth rule on proximal stem region that forces the stem to grow upwards, with only dendrite-dendrite repulsion force influencing other growth directions. Upon initiating first branching, dendrites start to seek for synaptic partner which introduce more options for branching. Beside immaturity of dendritic trees in area 1, the relatively stable trend in number of fronts and branch points in area 2 and area 3 on S0B can imply that dendritic trees growing from the same cell balance the elaboration of trees over tree areas. This assumption can be one role of the dendritic selection stage of Purkinje cell development because having stabilized elaboration in overall tree can avoid intensive competition in space and synapse in distal area, while leaving extra space and the resources in proximal area.

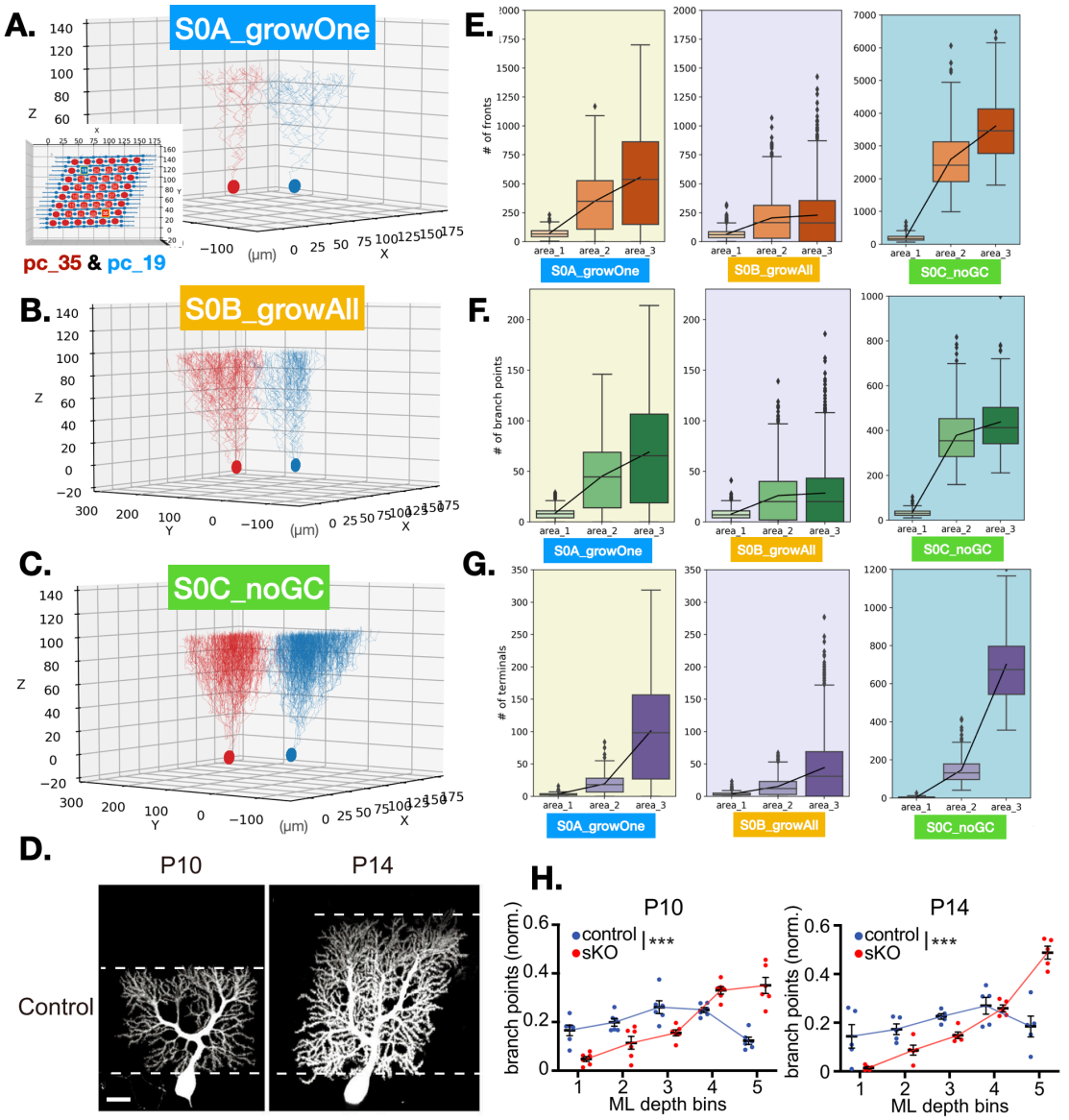

Figure 14. Morphology of winner trees by z-area. A) Two Purkinje cells (pc_35 in red and pc_19 in blue) at cycle 120/220 for scenario S0A are visualized. B) The same plot as A for scenario S0B. C) The same plot as A and B for scenario S0C. D) Purkinje cells from mice at postnatal day 10 and 14 (modified from Takeo et al. (2021). scale bar = 20µm E) Box plots to show number of fronts on 3 different z-axis area on winner trees of scenarios S0A, S0B, and S0C. Lower edge of the box plots indicate 25% of samples, middle line is median, and higher edge embrace 75% of samples. Vertical whiskers show maximum and minimum data points, and black dots are outliers. Lines connect the average number of fronts in each area. F) The same plots for number of branch points in 3 z-axis area. G) The same plots for number of terminals. H) Line plots showing branch points on different areas of each tree on P10 and P14 mice (modified from Takeo et al. (2021)); sKO: GluD2 parse knock out, ML: molecular layer.

3.3.1.4. Control growth scenario: conclusions

The simulation results from these scenarios suggest that the extended granule cell model provided enough numbers of parallel fibers for Purkinje cells in the model. There was a small discrepancy in morphology of the area proximal to the soma compared to the ones in observed in real systems, this was due to how the growth model was defined. However, these growth models indicated a role of excess trees growing from the same cell to established balanced dendritic tree morphology by competing for space and synapses. Also, the comparisons show that the physical presence of granule cells contributes to the distinct planar structure of Purkinje cell dendritic trees.

3.3.2. Results from 3 retraction scenarios

Results from 3 retraction scenarios of dendritic selection were compared, and the retraction scenario with a specific threshold on number of synapses with parallel fibers generated the largest number of synapses. By comparing with control growth scenarios, the additional role of dendritic retraction stage to reinforce elaboration of selected dendritic trees could be analyzed.

3.3.2.1. number of synapses and size of dendritic trees

The number of synapses and path length of winner trees corresponding to combinations of parameter sets in the retraction scenario 1 through 3 are shown in Figure 15 (A, B, C, and D). The size of the circles on plots represents max path length of the winner trees and had similar ranges for all scenarios. Although there was a high variance in the number of synapses generated for all scenarios, clearly organized color maps of different parameter sets could be made for scenario 1 and 3. The plots from scenario 2_1 by fronts and scenario 2_2 by synapses have 3 sets of the color map plots for each (one representative color map out of the 3 sets is shown for scenarios 2_1 and 2_2 in Figure 15 as B_1 and B_2). Since these scenarios have 3 control parameters, one parameter is fixed to check combinations of the other two. While for scenarios 1 and 3 clear trends were visible in the color maps, this was less the case for scenarios 2_1 and 2_2 that were noisier. Highest average number of synapses on winners for scenarios were as follows:

scenario 1: 522.71

(WholeCheck_cycle_1 = 90, WholeCheck_cycle_2 = 90+7)

scenario 2_1: 513.17

(Whole_1st = 300, 1st_f_th = 20, Whole_2nd = 400)

scenario 2_2: 517.76

(Whole_syn_1st = 90, 1st_s_th = 30, Whole_syn_2nd = 180)

scenario 3: 491.18

(Whole_signal_1st = 500, Whole_signal_2nd = 1,200)

Scenario 3 had a lower average number of synapses than other retraction scenarios, probably because thresholds based on synaptic input may sometimes select smaller trees. An important difference between the scenarios is that scenario 1 forces two phased retractions at fixed cycles, choosing first two winners and then the final winner based on relative numbers of synapses. In contrast, scenario 2_1, 2_2 and 3 uses the best parameters from scenario 1 to start checking for number of fronts, number of synapses, and signals respectively, and then choose relative retraction timings for every cell depending on their specific criteria.

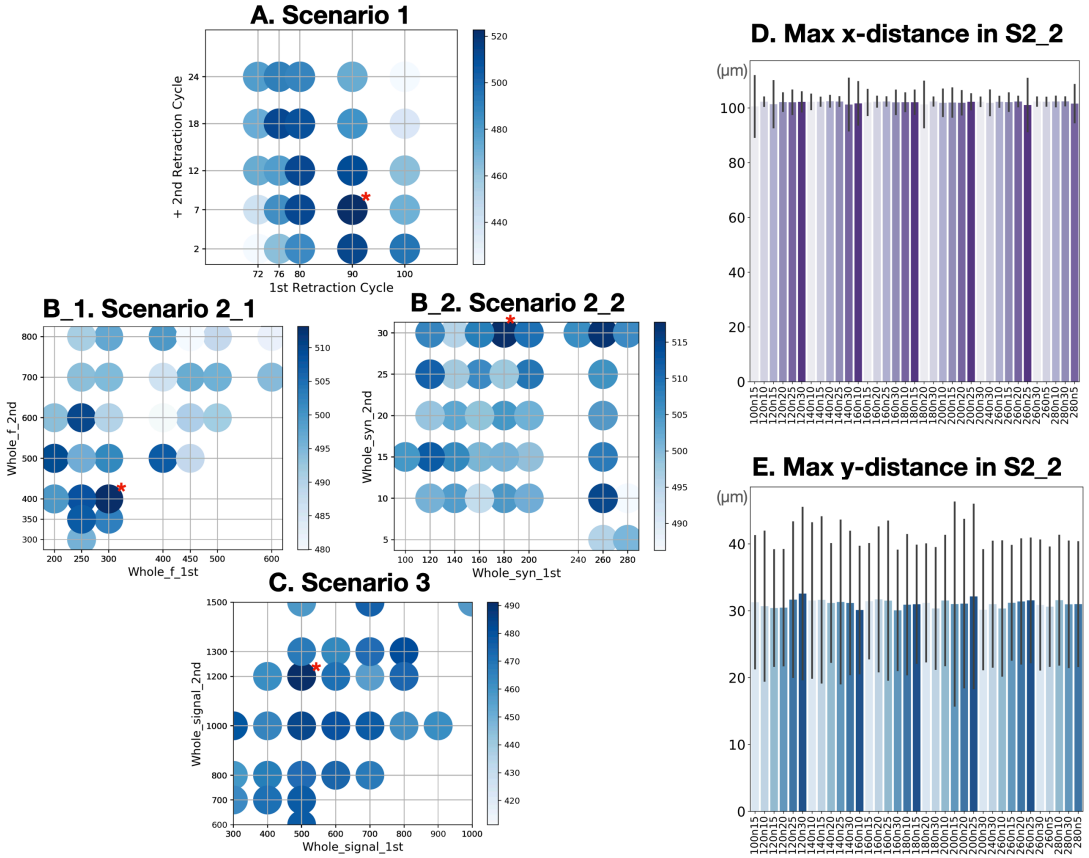

Figure 15. Number of synapses and arbor size of winner trees from retraction scenarios. A) The organized scatter map shows number of synapses by depth of colors with each combination of parameter sets. As shown in color bar, circles have darker color for increasing number of synapses. X-axis represents the first retraction cycle and y-axis shows number of cycles after a parameter for the first retraction cycle. For example, actual 2nd retraction cycle is 72 + 2 = 74 if the sample's 1st retraction cycle was 72, 2nd retraction cycle is 76 + 2 = 78 if its 1st retraction cycle was 76, and so on. The size of circles on the plot also represent average max path length of winner trees. The parameter set with the most numbers of synapses is marked with a red asterisk. B_1) A similar plot as A for scenario 2_1, but x- axis is Whole_1st threshold for fronts numbers, y-axis is for Whole_2nd threshold, and 1st_f_th is fixed at 20. B_2) A similar plot for scenario 2_2. X-axis shows Whole_2nd threshold for number of synapses, y-axis for 1st_s_th synapse threshold, and Whole_1st synapse threshold is fixed at 90. C) Similar plot for scenario 3. X-axis for Whole_signal_1st threshold and y-axis for Whole_signal_2nd threshold. A and C used 10 simulation samples for each parameter set, but three parameter sets with the largest number of synapses used additional 10 simulations. B_1, and B_2 used 20 simulation samples for each, and those trees that got 0 synapses but stayed until the end of simulation were excluded. D) Plotting average max x-distance of winner trees from one group of simulation sets in scenario 2_2 as a representative example for all scenarios. Vertical lines are error bars indicating standard deviations. E) The same plot as D, but for average max y-distance.

3.3.2.2. Morphology of winner trees

Max x-distance and y-distance of winner trees were also compared, but all selected trees in all scenarios of different parameter sets resulted in similar morphology in terms of the size (Figure 15D and E). As mentioned in the control scenario, x-distance of P120-180 mice is 82.9 ± 2.5 μm and y-distance is 13.9 ± 1.5 μm (Kim et al., 2011). Both x-distance and y-distance of winner trees in the retraction scenario is larger than observed, but they are still in acceptable range considering mouse Purkinje cell dendrites attain their final x-distance roughly by P13 in mice (C Sotelo & Dusart, 2009) and the y-distance around postnatal day 22 (Kaneko et al., 2011). Number of fronts, branch points, and terminals from all retraction scenarios also got similar trends (Figure 16). However, results from scenario 3 had a slightly smaller tree which correlated to their decrease in number of synapses. Box plots for number of fronts by area are not shown since there is a strong correlation between number of fronts and branch points in all 3 z-area (Figure 16A1). Compared with control scenarios S0A_growOne and S0B_growAll, winner trees from retraction scenarios tend to have larger numbers of fronts and branch points, which may imply a role of dendritic selection stage to elaborate dendritic trees. When comparing individual data of retraction timings (Figure 17), Purkinje cells in all scenarios experience the second retraction at similar simulation cycles. As one of simulation samples earned the most numbers of synapses in each scenario, there may be optimal timing to induce retractions to have the largest number of synapses although we do not have experimental data to compare numbers of synapses on dendritic trees.

In addition to the averaged data of multiple simulation samples, randomly selected individual synapse data in cycles and morphology of winner trees in single samples of each scenario are presented in Figure 18. There were obvious differences between the scenarios in the range of number of synapses in the winner trees. Scenario 2_1 clearly has a much lower variability, possibly due to selecting winners by tree size which may balance out structural differences. For other scenarios the distribution is different with scenario 1 showing a clear mean trend that is less obvious for scenarios 2_2 and 3; scenario 3 also has the largest variability overall.

Changes in numbers of fronts of winner trees per cycles in single sample (seed 11) of each scenario are presented in Figure 19 (A1, B1, C1, and D1). Each plot shows the data of randomly selected winner trees. There were obvious differences between the scenarios in the range of final front numbers. Scenario 2_1 clearly has a much lower variability, possibly due to selecting winners by tree size which may balance out structural differences. Scenario 3 has the largest variability overall for this sample. Number of fronts in all winner dendritic trees at cycle 140 for each scenario is also shown in Figure 19 (A2, B2, C2, and D2). Statistical differences of each data set by p values are also shown in the bottom of Figure 19. Purkinje cells in scenario 3, maybe the most realistic model among all the scenario, got a statistically significant characteristic of choosing relatively smaller trees as their primary dendrites.

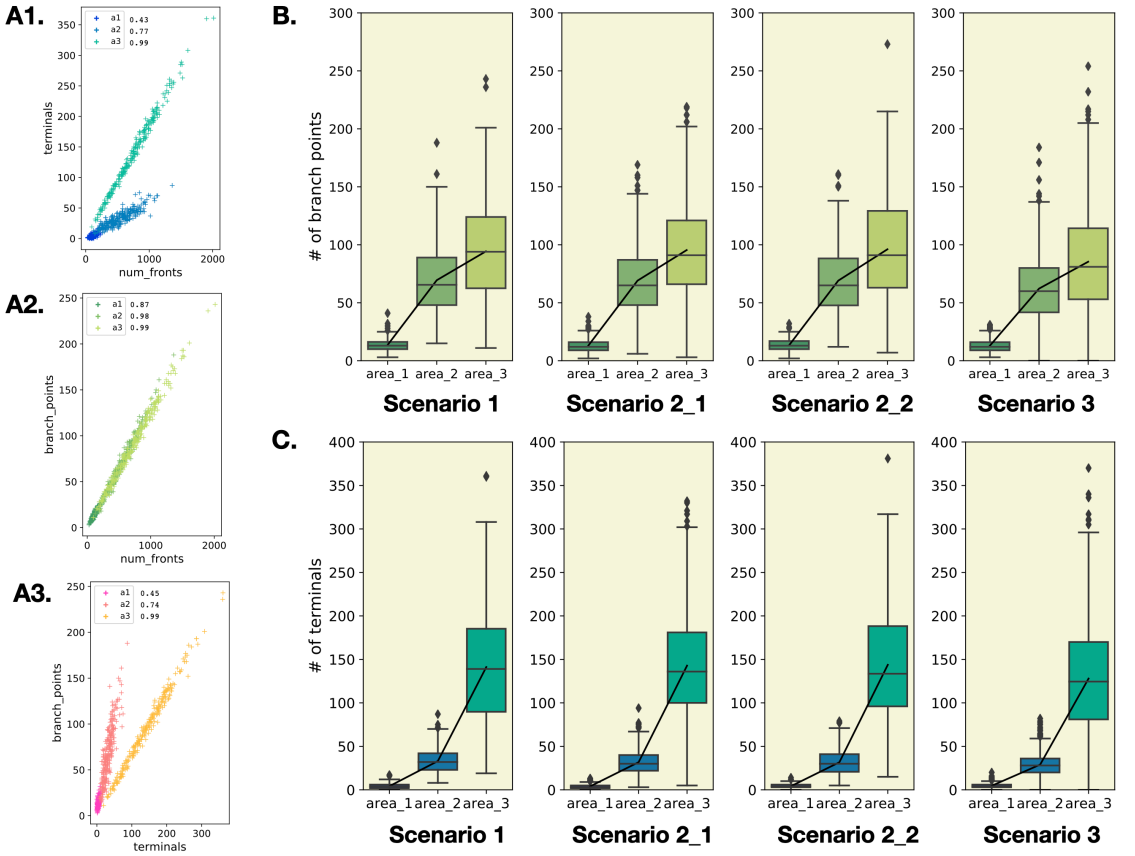

Figure 16. Morphology of winner trees by three z-area in retraction scenarios. A1) Scatter plots show correlation between results from number of fronts and terminals in 3 z area for scenario 1. a1: area 1 (bottom of a dendritic tree), a2: area 2 (middle of a tree), and a3: area 3 (upper part of a tree). Float values next by the legend are correlation coefficients of number of terminals and fronts in area 1, area 2, and area 3. A2) A similar plot as A1 for checking correlations between number of fronts and branch points in 3 areas for scenario 1 results. A3) A similar plot as A1 and A2 for terminals and branch points. B) Box plots to show number of branch points on 3 different z-axis area on winner trees of scenario S1, S2_1, S2_2 and S3. Lower edges of the box plots indicate 25% of samples, middle line is median, and higher edge embrace 75% of samples. Vertical whiskers show maximum and minimum data points, and black dots are out-liars. Line plots represents average branch points in each area. C) A similar plot as B for number of terminals.

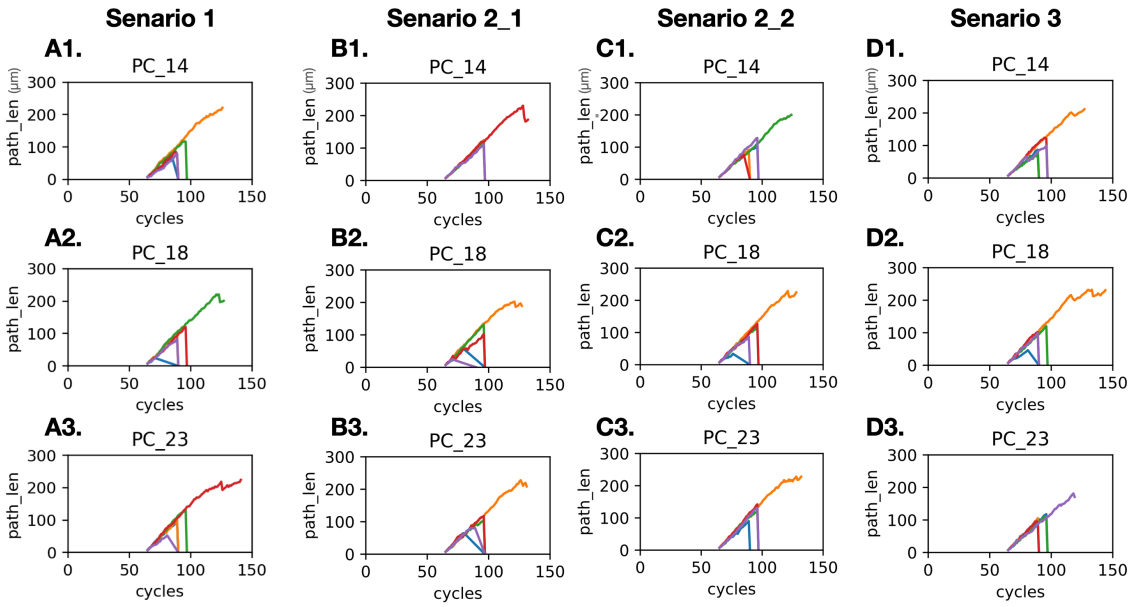

Figure 17. Change in path length with increasing cycles. A1-3) The plots show change in max path length of each candidate tree at every cycle with a different line color for each dendrite. Three Purkinje cells were randomly selected from one of 20 simulations in scenario 1. Since scenario 1 induce retractions at 2 fixed cycles, max path lengths of unselected trees dropped to 0 (retracted) at cycle 90 and 97. Two candidate trees in the sample (blue line on A2 and purple one on A3) could not fully grow as other trees and resulted in odd retraction lines. B1-3) Similar plots as A1-3 from one of 20 simulations in scenario 2_1. All cells skipped the first retraction because all the dendritic trees had a larger number of fronts than the given threshold (20 fronts for this case) when a cell reached the whole cell front number threshold (300 fronts). Then, a winner was chosen when a cell reached 2nd whole cell front number threshold (400 fronts). C1-3) Similar plots as A1-3 and A1-B from one of 20 simulations in scenario 2_2 whose 1st retraction thresholds for synapse numbers in each tree was 30 and in whole cell was 90, and whole cell threshold for 2nd retraction was 180 synapses. D1-3) Similar plots as others but from one of 20 simulations in scenario 3 whose 1st retraction threshold for signal in whole cell was 500 and 2nd was 12,00.

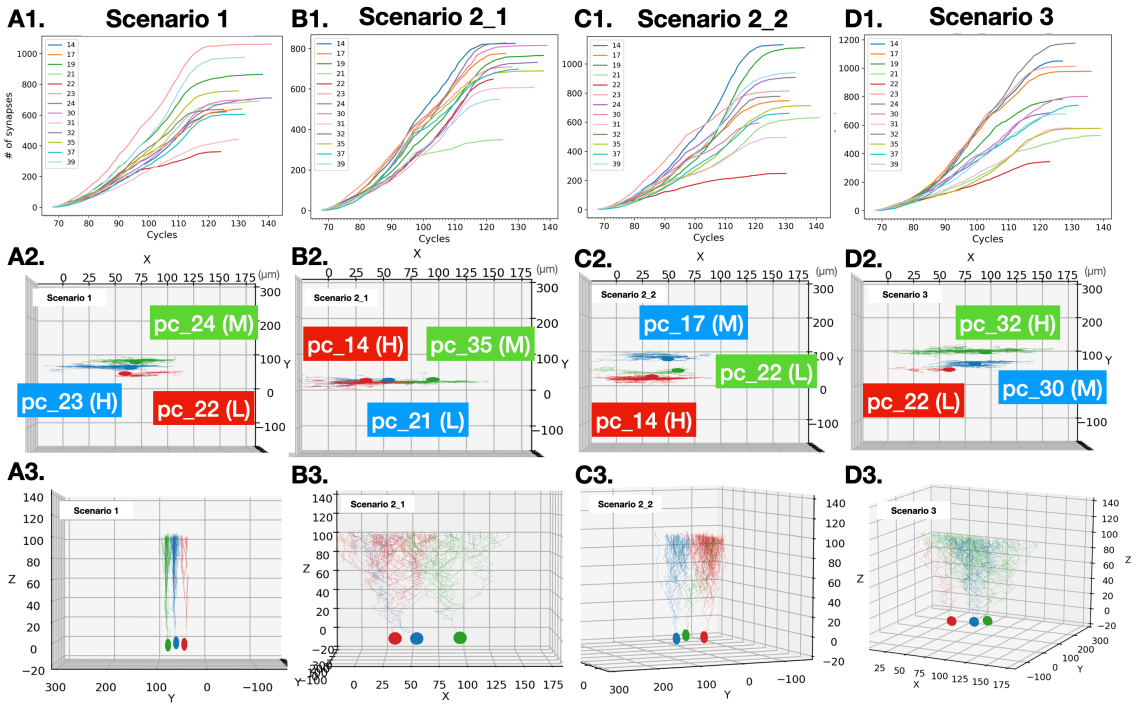

Figure 18. Morphology of individual winner trees from single samples in retraction scenarios. A1), B1), C1), and D1) A plot to show change in number of synapses at every simulation cycle in one of the simulations in each scenario. Plotted Purkinje cell samples are selected randomly, and numbers in legend corresponds to numbers in Purkinje cell location map on Figure 3.5D. A2), B2), C2), D2) Top view of selectively visualized Purkinje cells at cycle 220/220. Purkinje cells with highest (H), lowest (L), and somewhere in middle (M) number of synapses from A1-D1 plots were selected for each. A3), B3), C3), D3): Plots to show morphology of winner trees in A2-D2 from different directions. Scenario 1 data is from a seed 1 simulation of a parameter set with WholeCheck_cycle_1 = 90 and WholeCheck_cycle_2 = 90+7. Scenario 2_1 data is from a seed1 of a parameter set Whole_1st = 400, 1st_f_th = 20, and Whole_2nd = 500. Scenario 2_2 is from seed 1 of Whole_syn_1st = 90, 1st_s_th = 30, and Whole_syn_2nd = 160. Scenario 3 is from seed 1 of Whole_signal_1st = 10,000 and Whole_signal_2nd = 13,000.

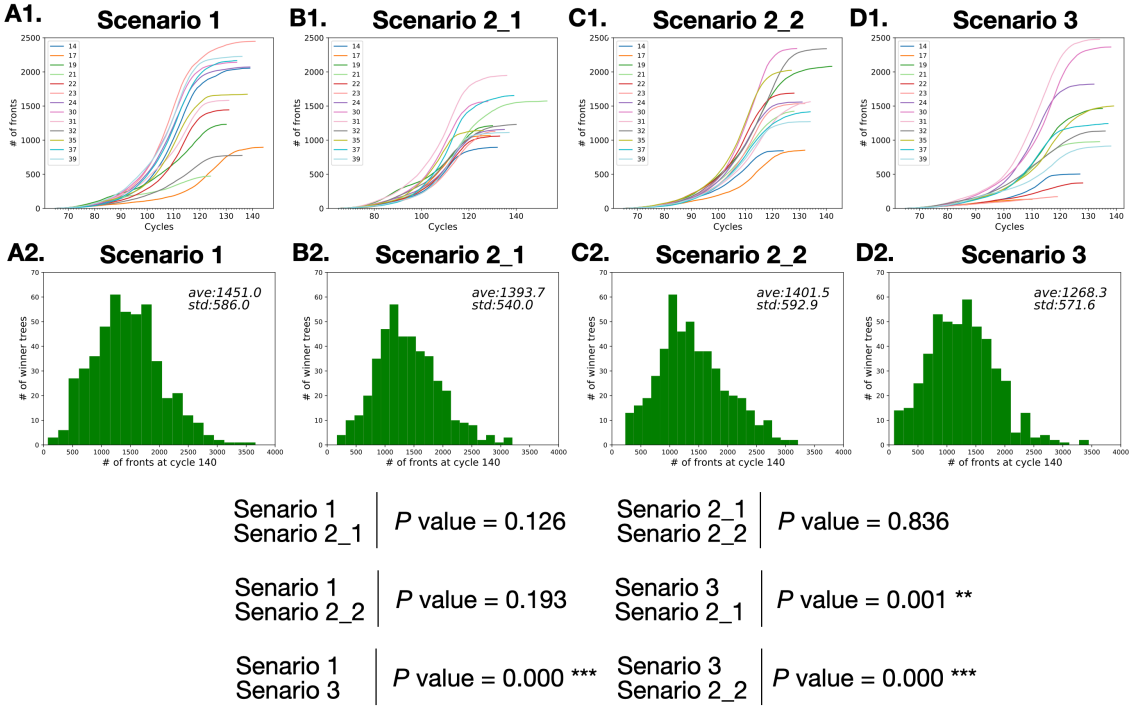

Figure 19. Variability of winner tree size in retraction scenarios. A1), B1), C1), and D1) A plot to show change in number of fronts at every simulation cycle in one of the simulations (seed 11) from the parameter sets that generated largest numbers of synapses in each scenario. Plotted Purkinje cell samples are selected randomly, and numbers in legend corresponds to numbers in Purkinje cell location map on Figure 3.5D. A2), B2), C2), D2) Histograms for numbers of fronts on winner trees from all 20 simulations in each scenario. Average and standard deviation of each data set is shown in each plot. P values for comparing each data set are listed at the bottom.

3.3.2.3. Retraction scenario: conclusions

When compared with tree morphology from control scenario, winner trees from retraction scenarios tend to have larger numbers of fronts and branch points that indicate a role of the selection process to elaborate primary dendritic trees. In terms of having opportunity to form larger numbers of synapses, common optimal timings of retractions were observed across all retraction scenarios. The comparisons of scenarios by two different definitions of maturations (scenario 2_1 by size vs. scenario 2_2 by synapses) showed that choosing winners by sizes of the trees might not be the best choice compared to directly choosing winners by the largest number of synapses. Also, when the selection was controlled by integrated synaptic signals (scenario 3), whose presynaptic partners gain mature average firing rate when they reach the bottom of the molecular layer, cells sometimes favored smaller trees as their primary dendrites.

4. Discussion

4.1. Summary of the main results

4.1.1. Granule Cell models

The number of cerebellar granule cells is too massive to obtain consensus measurements. However, the granule cell model of this project established a standard population at age P0 to 10 that could be simulated effectively. Also, the collisions observed in the model revealed how physically intensive the radial migrations and parallel fiber extensions are during cerebellar development. The expanded granule cell model increased the total number of parallel fibers in the main volume of the simulation. Although the number of parallel fibers in the model remained lower than expected in the biological system, the model provided enough numbers of free synapse locations for Purkinje cell models growing in them.

4.1.2. Purkinje cell models

A Purkinje cell growth model with continuous growths of all dendritic tree candidates on the same cell suggested that dendrite-dendrite repulsion may not be the main factor to keep its unique flat structure. Instead, the presence of parallel fibers to guide Purkinje cell dendritic growth was more important. Also, the Purkinje cell models suggested possible roles of the dendritic selection stage in facilitating sophistication of trees and in balancing a consistent elaboration of the vertical area of trees. Meanwhile, keeping multiple dendritic trees until later developmental stage may result in less elaborated winner trees. The model then explored detailed mechanisms of dendritic selection using 3 scenarios. While for retraction scenarios 1 and 3 clear trends were visible in the parameter maps for number of synapses in winner trees, this was less the case for scenarios 2_1 and 2_2 that were noisier. This may be due to the use of a fixed threshold for screening candidate trees at the first retraction stage. Using a relative threshold scheme, at least for the first retraction phase, might be more optimal for finding most efficient combinations of parameter sets to obtain larger number of synapses. Using the size of arbor as criteria of the winner selection did not necessary result in obtaining a larger number of synapses with parallel fibers. Rather, number of synapses itself may be the more important factor to win the selection. This trend also reflects the biological rule that the selection is not size dependent (personal communication, Prof. Yukari Takeo and Prof. Michisuke Yuzaki). Conversely, synaptic input reflecting network activity was less efficient as selection criteria because it sometimes favors relatively small dendritic trees.

4.2. Limitations of the models

4.2.1. Granule cell models

The largest difference between the models and biological systems is that cerebellar expansion during development was not implemented. The cerebellum undergoes a massive expansion, especially along the anterior-posterior plane (x-axis in the simulation cube) (Legué, Riedel, & Joyner, 2015) during 2 weeks after birth in mice (Altman, 1997). While the anterior-posterior plane in embryonic days 17.5 mouse has half the length of its molecular layer axis (z-axis in the cube), the anterior-posterior axis in postnatal mice expands 7.8 times longer than the molecular layer which also expands significantly (Legué et al., 2015). Therefore, this lack of volume expansion strongly affects crowding of cells, making it more difficult to manage migrations and growths of large cell populations.

There is also a difference in the process of extending parallel fibers during granule cell migration between the model and real neurons. In murine cerebellum, parallel fibers already extend during horizontal migration. However, because of NeuroDevSim limitations, the model extended parallel fiber axons after horizontal migration. The purpose of horizontal migration in biological system is unclear, but it might relate to granule cell allocation upon extension of the cortex (Consalez, Goldowitz, Casoni, & Hawkes, 2021), which is not implemented in the model. In the real cortex, it may be advantageous to already extend axons to preserve space for axonal expansion since the space just above horizontally migrating granule cells is filled with layers of proliferating granule cells, and it may be quite difficult to squeeze in to form new T-junctions. Since the model does not implement proliferations of granule cells, granule cells have free space to grow T-junctions above them, resulting in quite a high success rate of T-junction formation.

4.2.2. Purkinje cell models

For Purkinje cell models, apoptosis and reorganizations of soma positions in Purkinje cell layer were not simulated. Also, spiny dendrites and stem dendrites are not distinguished in the model. Finally, development only until P10 was simulated, excluding later growth of the winning dendritic trees from analysis.

4.3. Potential improvements and future directions of the models

In the model, all granule cells are homogeneous in that there is no zonal patterning by molecular phenotypes or birth orders. Such inhomogeneity in granule cells can be represented by, for example, 2 different types of molecular diffusions in the model to facilitate the zoning. Also, we can set different types of granule cell objects and assign different preferences in making synapses with distal or proximal regions of Purkinje cells' dendritic trees as observed (Dorgans et al., 2018; Gundappa-Sulur, De Schutter, & Bower, 1999). It is technically also possible to include granule cell proliferation, but in the absence of tissue expansion in the model this may not be useful. For the dendritic structure

of Purkinje cells, an additional growth algorithm to facilitate more elaboration of the proximal region of dendritic trees should be introduced to match the observed morphology. Also, the model needs to use a thicker outer wall of Purkinje cells to prevent edge effects since x-width of dendritic trees grow beyond the internal area of the Purkinje cell cluster.

Influence of dendritic trees growing from the same cell on morphology of the winning dendritic tree was observed in the model. There are interesting cases in retraction scenario 2 simulations, where some cells ended up with no dendritic trees due to too high thresholds, and having such soma only cells boosted the average number of synapses of winner trees in surrounding cells. These results were treated as outliers in the analysis, but it would be interesting to check specific influence of surrounding dendritic trees as environmental parameters separated from influence of dendritic trees from the same cell. Simulating later stages of development is also a compelling challenge. The comparison of different retraction scenarios suggests that the 1st retraction threshold is more likely to be specific for each cell. It is worth to confirm that the threshold for 2nd retractions works similarly. Moreover, the model assumed 2-phased dendritic retractions observed by Prof. Yukari Takeo, and it may be interesting to compare models with uni-phase or multiphase retraction schemes to explore advantages of having the 2-phases retraction system.

4.4. Contributions of the models

Experimentally inducing no granule cell environment in the cerebellar cortex can result in too many effects on its development like disturbing tissue expansions, molecular interactions, or development of neurons other than Purkinje cells. Our models enabled to observe the physical interactions of granule cell migrations and dendritic development of Purkinje cells without such constraints. This provided an indication for understanding well-known yet unexplained flat dendritic structure as being shaped by physical constraints of granule cells. Also, dendritic retraction scenario 3 reflected the preference for sometimes choosing smaller candidate tree as primary dendrite. If confirmed, this would indicate an involvement of the granule cell synaptic signal processing in the selection process of primary trees in Purkinje cells. Our computational work can be combined with experimental approaches to further explore the relationship between number of synapses and size of the dendritic trees. Experimental explorations on young Purkinje cells are still lacking, and it may be technically possible to mark synapses on the dendrites and counting them via microscopic images in vitro. Then, we can check for correlations between the number of synapses and size of the dendritic trees. This can also be combined with in vivo observations to obtain the data at specific timing of the developmental phase such as right after the dendritic selections. Obtaining data on the effect of synaptic input may be more challenging. This would be plausible only if synaptic plasticity is present in the young dendritic trees and if there is a reliable anatomical marker. Moreover, if tissue culture systems in early postnatal cerebellum is possible, we can test for signal activities in vitro like selectively activating synaptic input on one of the candidate trees and observe its effects on the selection. Lastly, the model is the first attempt to reproduce the development of main neurons in the cerebellar cortex with

detailed interactions between different types of neurons. The real-life cerebellum has evolved to be very complicated, therefore revealing this complexity by experimental procedures is obviously important. Modeling helps to re-organize and optimize the numerous information gained from live samples and facilitates to understand the bigger picture of how things work.

Bibliography

Altman, J. (1972). Postnatal development of the cerebellar cortex in the rat. III. Maturation of the components of the granular layer. *Journal of comparative Neurology, 145*(4), 465-513.

Altman, J. (1976). Experimental reorganization of the cerebellar cortex. V. Effects of X-irradiation schedules that allow or prevent cell acquisition after basket cells are formed. *Journal of comparative Neurology, 165*(1), 49-63.

Altman, J. (1997). Development of the cerebellar system. *Relation to its Evolution, Structure, and Functions.*

Armengol, J.-A., & Sotelo, C. (1991). Early dendritic development of Purkinje cells in the rat cerebellum. A light and electron microscopic study using axonal tracing in 'in vitro'slices. *Developmental brain research, 64*(1-2), 95-114.

Basson, M. A., & Wingate, R. J. (2013). Congenital hypoplasia of the cerebellum: developmental causes and behavioral consequences. *Frontiers in neuroanatomy, 7*, 29.

Berry, M., & Bradley, P. (1976). The growth of the dendritic trees of Purkinje cells in the cerebellum of the rat. *Brain research, 112*(1), 1-35.

Blazeski, R., & Mason, C. A. (1994). Cell-cell interactions influence survival and differentiation of purified Purkinje cells in vitro. *Neuron, 12*(2), 243-260.

Boukhtouche, F., Janmaat, S., Vodjdani, G., Gautheron, V., Mallet, J., Dusart, I., & Mariani, J. (2006). Retinoid-related orphan receptor α controls the early steps of Purkinje cell dendritic differentiation. *Journal of Neuroscience, 26*(5), 1531-1538.

Brodland, G. W. (2015). *How computational models can help unlock biological systems.* Paper presented at the Seminars in cell & developmental biology.

Butts, T., Green, M. J., & Wingate, R. J. (2014). Development of the cerebellum: simple steps to make a 'little brain'. *Development, 141*(21), 4031-4041.

Cerminara, N. L., Lang, E. J., Sillitoe, R. V., & Apps, R. (2015). Redefining the cerebellar cortex as an assembly of non-uniform Purkinje cell microcircuits. *Nature Reviews Neuroscience, 16*(2), 79-93.

Consalez, G. G., Goldowitz, D., Casoni, F., & Hawkes, R. (2021). Origins, development, and compartmentation of the granule cells of the cerebellum. *Frontiers in Neural Circuits, 14*, 88.

Das, G. D., Lammert, G. L., & McAllister, J. P. (1974). Contact guidance and migratory cells in the developing cerebellum. *Brain research, 69*(1), 13-29.

de Blas, A. L., & Cherwinski, H. M. (1985). The development of the Bergmann fiber palisades in the cerebellum of the normal rat and in the weaver mouse. *Brain research, 342*(2), 234-241.

De Schutter, E. (2022). Efficient simulation of neural development using shared memory parallelization. *bioRxiv*, 2022.2010.2017.512465. doi:10.1101/2022.10.17.512465

De Zeeuw, C. I., & Hoogland, T. M. (2015). Reappraisal of Bergmann glial cells as modulators of cerebellar circuit function. *Frontiers in cellular neuroscience, 9*, 246.

Dorgans, K., Demais, V., Bailly, Y., Poulain, B., Isope, P., & Doussau, F. (2018). Molecular and functional heterogeneity of cerebellar granule cell terminals expands temporal coding in molecular layer interneurons. *bioRxiv*, 338152.

Forbes, E. M., Thompson, A. W., Yuan, J., & Goodhill, G. J. (2012). Calcium and cAMP levels interact to determine attraction versus repulsion in axon guidance. *Neuron, 74*(3), 490-503.

Frascoli, F., Hughes, B. D., Zaman, M. H., & Landman, K. A. (2013). A computational model for collective cellular motion in three dimensions: general framework and case study for cell pair dynamics. *PloS one, 8*(3), e59249.

Fraser, S. E., & Perkel, D. H. (1990). Competitive and positional cues in the patterning of nerve connections. *Journal of neurobiology, 21*(1), 51-72.

Fujishima, K., Horie, R., Mochizuki, A., & Kengaku, M. (2012). Principles of branch dynamics governing shape characteristics of cerebellar Purkinje cell dendrites. *Development, 139*(18), 3442-3455.

Gadsdon, D. R., & Emery, J. L. (1976). Some quantitative morphological aspects of post-natal human cerebellar growth. *Journal of the Neurological Sciences, 29*(2-4), 137-148.

Goodhill, G. J., Gu, M., & Urbach, J. S. (2004). Predicting axonal response to molecular gradients with a computational model of filopodial dynamics. *Neural Computation, 16*(11), 2221-2243.

Graham, B. P., Lauchlan, K., & Mclean, D. R. (2006). Dynamics of outgrowth in a continuum model of neurite elongation. *Journal of computational neuroscience, 20*(1), 43-60.

Gundappa-Sulur, G., De Schutter, E., & Bower, J. M. (1999). Ascending granule cell axon: an important component of cerebellar cortical circuitry. *Journal of comparative Neurology, 408*(4), 580-596.

Harvey, R., & Napper, R. (1988). Quantitative study of granule and Purkinje cells in the cerebellar cortex of the rat. *Journal of comparative Neurology, 274*(2), 151-157.

Huang, C. m., Wang, L., & Huang, R. H. (2006). Cerebellar granule cell: ascending axon and parallel fiber. *European Journal of Neuroscience, 23*(7), 1731-1737.

Ito, M. (2006). Cerebellar circuitry as a neuronal machine. *Progress in neurobiology, 78*(3-5), 272-303.

Itoh, T., Sobue, G., Yasuda, T., Kimata, K., Mitsuma, T., & Takahashi, A. (1993). Geometric response to nerve growth factor is preserved in aged rat sensory neurons: a single-neuron culture study. *Neurobiology of aging, 14*(2), 167-176.

Jan, Y.-N., & Jan, L. Y. (2010). Branching out: mechanisms of dendritic arborization. *Nature Reviews Neuroscience, 11*(5), 316-328.

Kalinovsky, A., Boukhtouche, F., Blazeski, R., Bornmann, C., Suzuki, N., Mason, C. A., & Scheiffele, P. (2011). Development of axon-target specificity of ponto-cerebellar afferents. *PLoS biology, 9*(2), e1001013.

Kaneko, M., Yamaguchi, K., Eiraku, M., Sato, M., Takata, N., Kiyohara, Y., . . . Kengaku, M. (2011). Remodeling of monoplanar Purkinje cell dendrites during cerebellar circuit formation. *PloS one, 6*(5), e20108.

Keller, D., Erö, C., & Markram, H. (2018). Cell densities in the mouse brain: a systematic review. *Frontiers in neuroanatomy, 12*, 83.

Kim, J., Kwon, N., Chang, S., Kim, K.-T., Lee, D., Kim, S., . . . Hwu, Y. (2011). Altered branching patterns of Purkinje cells in mouse model for cortical development disorder. *Scientific reports, 1*(1), 1-7.

Komuro, H., Yacubova, E., Yacubova, E., & Rakic, P. (2001). Mode and tempo of tangential cell migration in the cerebellar external granular layer. *Journal of Neuroscience, 21*(2), 527-540.

Lange, W. (1975). Cell number and cell density in the cerebellar cortex of man and some other mammals. *Cell and tissue research, 157*(1), 115-124.

Leffler, S. R., Legué, E., Aristizábal, O., Joyner, A. L., Peskin, C. S., & Turnbull, D. H. (2016). A mathematical model of granule cell generation during mouse cerebellum development. *Bulletin of mathematical biology, 78*(5), 859-878.

Legué, E., Riedel, E., & Joyner, A. L. (2015). Clonal analysis reveals granule cell behaviors and compartmentalization that determine the folded morphology of the cerebellum. *Development, 142*(9), 1661-1671.

Leto, K., Arancillo, M., Becker, E. B., Buffo, A., Chiang, C., Ding, B., . . . Hatten, M. E. (2016). Consensus paper: cerebellar development. *The Cerebellum, 15*(6), 789-828.

Limperopoulos, C., Bassan, H., Gauvreau, K., Robertson, R. L., Sullivan, N. R., Benson, C. B., . . . Volpe, J. J. (2007). Does cerebellar injury in premature infants contribute to the high prevalence of long-term cognitive, learning, and behavioral disability in survivors? *Pediatrics, 120*(3), 584-593.

Luczak, A. (2006). Spatial embedding of neuronal trees modeled by diffusive growth. *Journal of neuroscience methods, 157*(1), 132-141.

Manto, M., Gruol, D. L., Schmahmann, J. D., Koibuchi, N., & Rossi, F. (2013). *Handbook of the cerebellum and cerebellar disorders* (Vol. 4): Springer.

McLean, D. R., van Ooyen, A., & Graham, B. P. (2004). Continuum model for tubulin-driven neurite elongation. *Neurocomputing, 58*, 511-516.

Merino-Casallo, F., Gomez-Benito, M. J., Juste-Lanas, Y., Martinez-Cantin, R., & Garcia-Aznar, J. M. (2018). Integration of in vitro and in silico models using Bayesian optimization with an application to stochastic modeling of mesenchymal 3D cell migration. *Frontiers in physiology*, 1246.

Miale, I. L., & Sidman, R. L. (1961). An autoradiographic analysis of histogenesis in the mouse cerebellum. *Experimental neurology, 4*(4), 277-296.

Miyata, M., Miyata, H., Mikoshiba, K., & Ohama, E. (1999). Development of Purkinje cells in humans: an immunohistochemical study using a monoclonal antibody against the inositol 1, 4, 5-triphosphate type 1 receptor (IP3R1). *Acta neuropathologica, 98*(3), 226-232.

Morrison, M. E., & Mason, C. A. (1998). Granule neuron regulation of Purkinje cell development: striking a balance between neurotrophin and glutamate signaling. *Journal of Neuroscience, 18*(10), 3563-3573.

Nagata, I., Ono, K., Kawana, A., & Kimura-Kuroda, J. (2006). Aligned neurite bundles of granule cells regulate orientation of Purkinje cell dendrites by perpendicular contact guidance in two-dimensional and three-dimensional mouse cerebellar cultures. *Journal of comparative Neurology, 499*(2), 274-289.

Nishiyama, J., Hayashi, Y., Nomura, T., Miura, E., Kakegawa, W., & Yuzaki, M. (2012). Selective and regulated gene expression in murine Purkinje cells by in utero electroporation. *European Journal of Neuroscience, 36*(7), 2867-2876.

Ono, K., Shokunbi, T., Nagata, I., Tokunaga, A., Yasui, Y., & Nakatsuji, N. (1997). Filopodia and growth cones in the vertically migrating granule cells of the postnatal mouse cerebellum. *Experimental brain research, 117*(1), 17-29.

Otero, J. J., Kalaszczynska, I., Michowski, W., Wong, M., Gygli, P. E., Gokozan, H. N., . . . Catacutan, F. P. (2014). Cerebellar cortical lamination and foliation require cyclin A2. *Developmental biology, 385*(2), 328-339.

Palkovits, M., Magyar, P., & Szentagothai, J. (1971). Quantitative histological analysis of the cerebellar cortex in the cat: I. Number and arrangement in space of the purkinje cells. *Brain research, 32*(1), 1-13.

Paňková, K., Rösel, D., Novotný, M., & Brábek, J. (2010). The molecular mechanisms of transition between mesenchymal and amoeboid invasiveness in tumor cells. *Cellular and molecular life sciences, 67*(1), 63-71.

Pichitpornchai, C., Rawson, J., & Rees, S. (1994). Morphology of parallel fibres in the cerebellar cortex of the rat: an experimental light and electron microscopic study with biocytin. *Journal of comparative Neurology, 342*(2), 206-220.

Poulain, F. E., Chauvin, S., Wehrlé, R., Desclaux, M., Mallet, J., Vodjdani, G., . . . Sobel, A. (2008). SCLIP is crucial for the formation and development of the Purkinje cell dendritic arbor. *Journal of Neuroscience, 28*(29), 7387-7398.

Rahimi-Balaei, M., Bergen, H., Kong, J., & Marzban, H. (2018). Neuronal migration during development of the cerebellum. *Frontiers in cellular neuroscience, 12*, 484.

Ramón Y Cajal, S. (1911). Histologie du syst6me nerveux de l'homme et des vert6br6s. 2 vol. *Madrid: CSIC*.

Ribeiro, F., Gómez-Benito, M., Folgado, J., Fernandes, P., & García-Aznar, J. (2017). Computational model of mesenchymal migration in 3D under chemotaxis. *Computer methods in BiomeChaniCs and BiomediCal engineering, 20*(1), 59-74.

Rio, C., Rieff, H. I., Qi, P., & Corfas, G. (1997). Neuregulin and erbB receptors play a critical role in neuronal migration. *Neuron, 19*(1), 39-50.

Roccasalvo, I. M., Micera, S., & Sergi, P. N. (2015). A hybrid computational model to predict chemotactic guidance of growth cones. *Scientific reports, 5*(1), 1-17.

Shiga, T., Ichikawa, M., & Hirata, Y. (1983). Spatial and temporal pattern of postnatal proliferation of Bergmann glial cells in rat cerebellum: an autoradiographic study. *Anatomy and embryology, 167*(2), 203-211.

Sillitoe, R. V. (2016). Mossy fibers terminate directly within Purkinje cell zones during mouse development. *The Cerebellum, 15*(1), 14-17.

Simpson, H. D., & Goodhill, G. J. (2011). A simple model can unify a broad range of phenomena in retinotectal map development. *Biological cybernetics, 104*(1), 9-29.

Sotelo, C. (2004). Cellular and genetic regulation of the development of the cerebellar system. *Progress in neurobiology, 72*(5), 295-339.

Sotelo, C., & Arsenio-Nunes, M. (1976). Development of Purkinje cells in absence of climbing fibers. *Brain research, 111*(2), 389-395.

Sotelo, C., & Dusart, I. (2009). Intrinsic versus extrinsic determinants during the development of Purkinje cell dendrites. *Neuroscience, 162*(3), 589-600.

Squire, L., Berg, D., Bloom, F. E., Du Lac, S., Ghosh, A., & Spitzer, N. C. (2012). *Fundamental neuroscience*: Academic press.

Steen, A.-B. (2006). *Quantitative Morphological Analyses of the striatum and cerebellum of Tenascin-R deficient mice.* Staats-und Universitätsbibliothek Hamburg Carl von Ossietzky,

Sturrock, R. (1989). Changes in neuron number in the cerebellar cortex of the ageing mouse. *Journal fur Hirnforschung, 30*(4), 499-503.

Takeda, T., & Maekawa, K. (1989). Transient direct connection of vestibular mossy fibers to the vestibulocerebellar Purkinje cells in early postnatal development of kittens. *Neuroscience, 32*(1), 99-111.

Takeo, Y. H., Shuster, S. A., Jiang, L., Hu, M. C., Luginbuhl, D. J., Rülicke, T., . . . Ganguli, S. (2021). GluD2-and Cbln1-mediated competitive interactions shape the dendritic arbors of cerebellar Purkinje cells. *Neuron, 109*(4), 629-644. e628.

Talkenberger, K., Cavalcanti-Adam, E. A., Voss-Böhme, A., & Deutsch, A. (2017). Amoeboid-mesenchymal migration plasticity promotes invasion only in complex heterogeneous microenvironments. *Scientific reports, 7*(1), 1-12.

Tanaka, M., Yanagawa, Y., Obata, K., & Marunouchi, T. (2006). Dendritic morphogenesis of cerebellar Purkinje cells through extension and retraction revealed by long-term tracking of living cells in vitro. *Neuroscience, 141*(2), 663-674.

Tavano, A., Grasso, R., Gagliardi, C., Triulzi, F., Bresolin, N., Fabbro, F., & Borgatti, R. (2007). Disorders of cognitive and affective development in cerebellar malformations. *Brain, 130*(10), 2646-2660.

Torben-Nielsen, B., & De Schutter, E. (2014). Context-aware modeling of neuronal morphologies. *Frontiers in neuroanatomy, 8*, 92.

van Pelt, J., Graham, B. P., & Uylings, H. B. (2003). Formation of dendritic branching patterns. *Modeling neural development*, 75-94.

Vogel, M. W., Sunter, K., & Herrup, K. (1989). Numerical matching between granule and Purkinje cells in lurcher chimeric mice: a hypothesis for the trophic rescue of granule cells from target-related cell death. *Journal of Neuroscience, 9*(10), 3454-3462.

Weiss, G. M., & Pysh, J. (1978). Evidence for loss of Purkinje cell dendrites during late development: a morphometric Golgi analysis in the mouse. *Brain research, 154*(2), 219-230.

Zaman, M. H., Kamm, R. D., Matsudaira, P., & Lauffenburger, D. A. (2005). Computational model for cell migration in three-dimensional matrices. *Biophysical journal, 89*(2), 1389-1397.

Zanjani, H., Vogel, M., Delhaye-Bouchaud, N., Martinou, J., & Mariani, J. (1997). Increased inferior olivary neuron and cerebellar granule cell numbers in transgenic mice overexpressing the human Bcl-2 gene. *Journal of neurobiology, 32*(5), 502-516.

Zecevic, N., & Rakic, P. (1976). Differentiation of Purkinje cells and their relationship to other components of developing cerebellar cortex in man. *Journal of comparative Neurology, 167*(1), 27-47.

Zhu, J., & Mogilner, A. (2016). Comparison of cell migration mechanical strategies in three-dimensional matrices: a computational study. *Interface focus, 6*(5), 20160040.

Zubler, F., & Douglas, R. (2009). A framework for modeling the growth and development of neurons and networks. *Frontiers in computational neuroscience, 3*, 25.